

1 **Diagnostic calibration of a hydrological model in a mountain**
2 **area by hydrograph partitioning**

3 Z. H. He¹, F. Q. Tian^{1*}, H. V. Gupta², H. C. Hu¹, H. P.Hu¹

4

5

6 1. State Key Laboratory of Hydrosience and Engineering, Department of Hydraulic
7 Engineering, Tsinghua University, Beijing 100084, China

8 2. Department of Hydrology and Water Resources, The University of Arizona, Tucson,
9 Arizona, 85721, USA

10

11 *Corresponding author information:

12 Email: tianfq@tsinghua.edu.cn

13 Tele: +86 010 6277 3396

14 Fax: +86 010 6279 6971

15

16

17

18 Manuscript submitted to Hydrology and Earth System Sciences

19 2015.02.16

20 **Abstract**

21 Hydrological modeling can exploit informative signatures extracted from long time sequences
22 of observed streamflow for parameter calibration and model diagnosis. In this study we
23 explore the diagnostic potential of hydrograph partitioning for model calibration in mountain
24 areas, where meltwater from snow and glaciers are important sources for river runoff (in
25 addition to rainwater). We propose an index-based method to partition the hydrograph
26 according to dominant runoff water sources, and a diagnostic approach to calibrate a
27 mountain hydrological model. First, by accounting for the seasonal variability of precipitation
28 and the altitudinal variability of temperature and snow/glacier coverage, we develop a set of
29 indices to indicate the daily status of runoff generation from each type of water source (i.e.,
30 glacier meltwater, snow meltwater, rainwater, and groundwater). Second, these indices are
31 used to partition a hydrograph into four parts associated with four different combinations of
32 dominant water sources (i.e., groundwater, groundwater + snow meltwater, groundwater +
33 snow meltwater+ glacier meltwater, groundwater + snow meltwater + glacier meltwater +
34 rainwater). Third, the hydrological model parameters are grouped by the associated runoff
35 sources, and each group is calibrated to match the corresponding hydrograph partition in a
36 stepwise and iterative manner. Similar to use of the regime curve to diagnose seasonality of
37 streamflow, the hydrograph partitioning curve based on a dominant runoff water source (more
38 briefly called the partitioning curve, not necessarily continuous) can serve as a diagnostic
39 signature that helps relate model performance to model components. The proposed methods
40 are demonstrated via application of a semi-distributed hydrological model (THREW) to the
41 Tailan River basin (1324 km²) in the Tianshan Mountain of China. **Results show that the
42 proposed calibration approach performed reasonably well. Cross validation and comparison to
43 an automatic calibration method indicated its robustness.**

44 **1 Introduction**

45 **1.1 Background**

46 Parameter calibration has been singled out as one of the major issues in the application
47 of hydrological models (Johnston and Pilgrim, 1976; Gupta and Sorooshian, 1983; Beven and
48 Binley, 1992; Boyle *et al.*, 2000). Commonly, one or more objective functions are selected as
49 criteria to evaluate the similarity between observed and simulated hydrographs (Nash and
50 Sutcliffe, 1970; Brazil, 1989; Gupta *et al.*, 1998; van Griensven and Bauwens, 2003). As
51 model complexity increases, parameter dimensionality also increases significantly, which
52 makes it much more difficult to calibrate model parameters manually. For this reason,
53 automatic calibration procedures have been developed to identify the optimal parameter set
54 (Gupta and Sorooshian, 1985; Gan and Biftu, 1996; Vrugt *et al.*, 2003a,b). However, due to
55 limitations in process understanding and measurement technologies, one can find different
56 parameter sets within a chosen space that may acceptably reproduce the observed aspects of
57 the catchment system (Sorooshian and Gupta, 1983; Beven and Freer, 2001). This
58 phenomenon, which has been called “equifinality”, causes uncertainty in simulation and
59 prediction (Duan *et al.*, 1992; Beven, 1993, 1996), and highlights the need for methods that
60 are powerful enough to ‘diagnostically’ evaluate and correct models, i.e., that are capable of
61 indicating to what degree a realistic representation of the real world has been achieved and
62 pointing towards how the model should be improved (Spear and Hornberger, 1980; Gupta *et al.*,
63 1998, 2008).

64 Traditional regression-based model evaluation strategies (e.g., based on the use of Mean
65 Squared Error or Nash Sutcliffe Efficiency as performance criteria) are demonstrably poor in
66 their ability to identify the roles of various model components or parameters in the model
67 output (Van Straten and Keesman, 1991; Zhang *et al.*, 2008; Gupta *et al.*, 2008; Yilmaz *et al.*,
68 2008; Hingray *et al.*, 2010), which is due in part to the loss of meaningful information when
69 projecting from the high dimension of the data set (like hydrograph) down to the low (often
70 one) dimension of the measure (Yilmaz *et al.*, 2008; Gupta *et al.*, 2009). A diagnostic
71 evaluation method should match the number of unknowns (parameters) with the number of
72 pieces of information by making use of multiple measures of model performance (Gupta *et al.*,
73 1998, 2008, 2009; Yilmaz *et al.*, 2008). One way to exploit hydrological information is to

74 analyze the spatiotemporal characteristics of hydrological variables that can be related to
75 specific hydrological processes in the form of “signature indices”(Richter *et al.*, 1996;
76 Sivapalan *et al.*, 2003; Gupta *et al* 2008, Yilmaz *et al.*, 2008). Ideally, a “signature” should
77 represent some “invariant” property of the system, be readily identifiable from available data,
78 directly reflect some system function, and be maximally related to some “structure” or
79 “parameter” in the model.

80 Attention to hydrological signatures, therefore, constitutes the natural basis for model
81 diagnosis (Gupta *et al.*, 2008). Placed in this context, the body of literature on the topic is
82 indeed large. Jothityangkoon *et al.* (2001) proposed a downward approach to evaluate the
83 model’s performance against appropriate signatures at progressively refined time scale.
84 Signatures that govern the evaluation of model complexity are the inter-annual variability,
85 mean monthly variation in runoff (called regime curve), and the flow duration curve (FDC).
86 Farmer *et al.* (2003) evaluated the climate, soil and vegetation controls on the variability of
87 water balance through four signatures: gradient of the annual yield frequency graph, average
88 yield over many years for each month, FDC, and magnitude and shape of the hydrograph.
89 Shamir *et al.* (2005a) described a parameter estimation method based on hydrograph
90 descriptors (total flow, range between the extreme values, monthly rising limb density of the
91 hydrograph, monthly maximum flow and negative/positive change) that characterize
92 dominant streamflow patterns at three timescales (monthly, yearly, and record extent).
93 Detenbeck *et al.* (2005) calculated several hydrologic indices including daily flow indices
94 (mean, median, coefficient of variation, and skewness), overall flood indices (flood frequency,
95 magnitude, duration, and flood timing of various levels), low flow variables (mean annual
96 daily minimum), and ranges of flow percentiles to study the relationship of the streamflow
97 regime to watershed characteristics. Shamir *et al.* (2005b) presented two streamflow indices
98 to describe the shape of the hydrograph (rising/declining limb density, i.e., RLD and DLD)
99 for parameter estimation in 19 basins of United States. Yadav *et al.* (2007) used similarity
100 indices and hydrological signatures (runoff ratio and slope of the FDC) to classify catchments.
101 Westerberg *et al.* (2011) selected several evaluation points on the FDC to calibrate models,
102 and compared two selection methods to evaluate their effects on parameter calibration.

103 Generally, the reported signatures have the following two characteristics: (1) they

104 concentrate on the extraction of hydrologically meaningful information contained in
105 hydrographs, and (2) they focus on either an entire study period or a special continuous
106 section of the entire period. They have occasionally considered temporal variability of runoff
107 components and dominance of different runoff sources during different periods (e.g., the
108 seasonal switching of runoff sources discussed in Tian *et al.*, 2012). However, a hydrograph
109 could be dominated by various components or water sources at different response times
110 (Haberlandt *et al.*, 2001; Eder *et al.*, 2005). Within this in mind, a few studies have explored
111 the use of hydrological information in time dimension for stepwise calibration. For example,
112 Schaepli *et al.* (2005) presented a stepwise calibration method for 7 parameters in a high
113 mountainous area: snow and ice melt degree-day factors were conditioned by mass balance,
114 slow reservoir parameters were determined by base flow, reservoir coefficients were
115 calibrated by summer runoff, and the direct runoff coefficient was used to control discharge
116 during precipitation events. Another notable example is Hingray *et al.* (2010), in which the
117 authors estimated the value of snowmelt degree-day factor in a mountain basin by
118 progressively minimizing the differences between observed and simulated values of different
119 magnitude hydrographs. There are also many other follow up studies.

120 In mountain areas, streamflow is composed of both snow/glacier meltwater and
121 rainwater. The energy-based and temperature-index models are two principal approaches to
122 simulate snow and glacier melt (Rango and Martinec, 1979; Howard, 1996; Kane *et al.*, 1997;
123 Singh *et al.*, 2000; Fierz *et al.*, 2003). To describe significant heterogeneity of temperature,
124 precipitation, snow, and glacier, distributed hydrological models are generally used for
125 precipitation-runoff modeling in mountain regions (Daly *et al.*, 2000; Klok *et al.*, 2001 etc.).
126 Also, the utilization of remotely sensing products of precipitation and snow cover data in the
127 mountain runoff modeling has become more popular in recent years (Swamy and Brivio, 1997;
128 Akyurek *et al.*, 2011; Liu *et al.*, 2012 etc.). Most of these studies report sound simulation
129 results. However, the need to develop an appropriate calibration strategy for
130 precipitation-runoff modeling in mountain areas remains a key issue for two reasons: first, the
131 hydrological processes are usually more complex (with snow/glacier melt and possibly soil
132 freezing/thawing) than those in warmer areas, which implies a larger dimension of parameter
133 (R^p) in the corresponding hydrological model; second, measured data set useful for model

134 identification is usually limited due to a sparse gauge network, which produces a small
135 measurement dimension (R^M) far lower than R^P . To address this problem, related studies are
136 putting effort into two directions. One is to reduce the calibrated R^P by estimating some of the
137 parameters based on basin characteristics *a priori*. For example, Gurtz *et al.* (1999) proposed
138 a parameterization method based on elevation, slope and shading derived from basin terrain.
139 Gomez-Landesa and Rango (2002) obtained model parameters of ungauged basins from
140 gauged basins by basin size, proximity of location, and shape similarities. Eder *et al.* (2005)
141 estimated most of the parameters *a priori* from basin physiography before an automatic
142 calibration was applied. The parameterization method may involve some uncertainties but be
143 useful for the determination of insensitive parameters.

144 The second direction is to exploit hydrological information from implicit measure data.
145 For instance, Dunn and Colohan (1999) used baseflow data as additional criteria for model
146 evaluation. Mendoza *et al.* (2003) exploited recession-flow data to estimate hydraulic
147 parameters. Stahl *et al.* (2008) used glacier mass balance information combined with stream
148 hydrographs to constrain melt factors. Huss *et al.* (2008) used annual ice volume change data
149 for optimizing melt and radiation factors, and glacier equilibrium line altitude for
150 precipitation correction factors. Schaepli and Huss (2011) integrated the seasonal information
151 of point glacier mass balance for model calibration by modifying the GSM-SOCONT model.
152 Jost *et al.* (2012) introduced glacier volume loss calculated by high-resolution digital
153 elevation models to calibrate hydrologic model. Knowledge acquired from the
154 aforementioned research indicates that the use of additional information (e.g., baseflow,
155 recession flow, and glacier mass balance) can effectively help reduce parameter uncertainty
156 by significantly expanding R^M .

157 However, glacier mass data and baseflow data are usually not available in some
158 mountain basins. In these cases, hydrograph partitioning is another possible way to exploit
159 information from available data. Information about dominant hydrological processes
160 contained in a hydrograph can be extracted by hydrograph partitioning or separation; this has
161 long been a topic of interest in hydrology. Several different kinds of methods have been
162 proposed (Pinder and Jones, 1969; McCuen, 1989; Nathan, 1990; Arnold *et al.*, 1995, 1999;
163 Vivoni *et al.*, 2007), which can generally be classified into graphical methods, analytical

164 methods, empirical methods, geochemical methods and automated program techniques
165 (Nejadhashemi *et al.*, 2009). Most of them primarily focus on the partitioning of baseflow and
166 are not capable of identifying more than two components. With the advent of isotope methods,
167 multi-component hydrograph separation models have been developed. However, these models
168 need be run for an extended period of time (usually a minimum of one hydrologic year) for
169 the assumption that the isotopes of components are conserved to hold (Hooper and
170 Shoemaker, 1986) and call for volumes of field data that are seldom available in poorly
171 gauged and difficult to access mountain basins.

172 **1.2 Objectives and Scope**

173 This paper explores the benefits of partitioning the hydrograph into several parts, each
174 related to one combination of dominant water sources for runoff generation. The parameter
175 group controlling each type of runoff generation is then calibrated using the corresponding
176 partitioning hydrographic curves via a stepwise approach, and model deficiencies are
177 diagnosed by evaluating the model simulations associated with each partitioning curve (as a
178 diagnostic signature). We demonstrate the potential of this approach in a mountain area where
179 streamflow is the result of complex runoff generation processes arising from combinations of
180 storm events and snow/glacier melt. The influence of each type of water source (groundwater,
181 snow meltwater, glacier meltwater, or rainwater) varies in time and can be determined by an
182 analysis of the dynamic spatiotemporal information in the available data series.

183 The paper is organized as follows. Section 2 contains a description of the geographic
184 and hydrological characteristics of the study basin, including the main data sources and data
185 preprocessing. Section 3 details the proposed method of hydrograph partitioning and
186 parameter calibration based on a semi-distributed model coupled with the temperature-index
187 method. Section 4 presents the results and discusses the possible sources of uncertainty.
188 Section 5 provides a summary of this study and discusses further applications of the
189 partitioning strategy.

190 **2 Study Area and Data**

191 **2.1 Overview of the Study Area**

192 The study mountain area (Tailan River basin, TRB) is on the south slope of the Tianshan
193 Mountain (one of the highest mountain areas in China) in the Xinjiang Uygur Autonomous

194 Region of China and extends from 41° 35'N to 42° 05' N and 80° 04'E to 80° 35'E, covering a
195 drainage area of 1324 km².Elevation ranges from 1600 m to 7100 m a.s.l. with an average
196 value as high as 4100 m a.s.l. Precipitation occurs mainly in summer and rarely in winter, and
197 winter precipitation always comes in the form of snowfall. Snow coverage accumulates in
198 winter and ablates from spring into late summer when it melts away completely; the snow
199 coverage dynamics can be obtained from MODIS data (see Figure 4).The basin is highly
200 glacierized with approximately 33% of the basin area covered by glacier ice (see Figure 1).
201 The glacier coverage stretches from approximately 3000 m to 7100 m a.s.l. and exists mainly
202 at an altitude range of 4000 m to 5000 m a.s.l. Glacier melt and snowmelt form runoff as long
203 as the temperature rises above a certain threshold and provide primary sources for
204 downstream discharge.

205 TRB is a heavily studied mountain watershed in northwestern China. The relevant
206 literature(Kang and Zhu, 1980; Shen *et al.*, 2003; Xie *et al.*, 2004; Gao *et al.*, 2011; Sun *et al.*,
207 2012) are reviewed below, and the main conclusions about the hydrometeorological
208 characteristics are summarized as follows:

209 (1) The climate presents strong altitudinal variability. The mean annual precipitation in
210 higher mountain areas is approximately 1200 mm (Kang *et al.*, 1980), while it is
211 approximately only 180 mm in the outlet plain area (Xie *et al.*, 2004). The mean annual
212 temperature ranges from below 0°C in mountain areas to approximately 9°C at the basin
213 outlet (Sun *et al.*, 2012).

214 (2) Meltwater is the principal source of streamflow. Snow and glacier meltwater account
215 for approximately 63% of the annual runoff (Kang *et al.*, 1980). The contribution of rainwater
216 is relatively lower and occurs mainly in the storm rain period (May to September) (Xie *et al.*,
217 2004). Groundwater baseflow is smaller but dominates the streamflow in the winter (January,
218 February and December), during which either rainfall or melt rarely occur (Kang *et al.*, 1980).

219 (3) The TRB river network is a simple fan system. Given large topographic drop and
220 moderate drainage area, the runoff concentration time is no longer than one day (Xie *et al.*,
221 2004). Melting and falling water can quickly flow into the main channel and reach the basin
222 outlet.

223 2.2 Data & Preprocessing

224 The Tailan gauging station (THS, 1602 m a.s.l.) is located the outlet of the watershed,
225 where runoff, precipitation and temperature have been measured since 1957. To collect
226 temperature and precipitation data at higher elevation, two automatic weather stations (AWS,
227 product type TRM-ZS2) were set up in June 2011 (i.e., XT AWS, at 2116 m a.s.l. and TG
228 AWS, at 2381 m a.s.l.). This relatively short record (from July 1, 2011-December 31, 2012)
229 was used to estimate the lapse rate of precipitation and temperature (see below). The Bingtan
230 automatic weather station (BT AWS, at 3950 m a.s.l.) located in an adjacent catchment
231 (Kumalak basin) was used to validate the estimated temperature lapse rates. A digital
232 elevation model (DEM) with a spatial resolution of 30 m was provided by the International
233 Scientific & Technical Data Mirror Site, Computer Network Information Center of the
234 Chinese Academy of Sciences (<http://www.gscloud.cn>). Remotely sensed snow cover area
235 (SCA) data were downloaded from the MODIS website; the MOD10A2 and MYD10A2
236 products were used, both of which have a spatial resolution of 500m and a temporal
237 resolution of eight-days. Daily snow cover data was obtained by linear interpolation of the
238 eight-day data. The China Glacier Inventory (CGI) (Shi, 2008) was used to derive glacier
239 coverage in the TRB. In our experience, most of the snow melts away after the warm summer
240 period and the lowest snow/ice coverage in the year should, therefore, be roughly equal to the
241 glacier coverage. Based on an analysis of filtered MODIS SCA (see Sect. 2.2.3), the lowest
242 values of snow/ice coverage in the study period (2003-2012) are almost the same, which
243 indicates that TRB glacier coverage is relatively stable during the study period. The DEM,
244 river system, gauging stations and glacier distribution are shown in Fig.1.

245 2.2.1 Temperature Lapse Rate

246 Altitudinal distribution of temperature can be estimated through the lapse rate (Rango and
247 Martinec, 1979; Tabony, 1985). According to Aizen *et al.* (2000), rates of temperature
248 decrease with increasing elevation are quite different in various months, and ignoring this
249 difference may lead to significant errors in the simulation of snow accumulation and melt.
250 The lapse rate was therefore estimated for each month. Temperature variations with altitude
251 can be estimated by the following equation, i.e.:

252
$$T = T_o + T_p \cdot (H - h) \quad (1)$$

253 where, T_o is the temperature value at low altitude (THS in this study), and T_p is the
 254 temperature lapse rate (usually negative), H and h are the elevation values at high and low
 255 positions, i.e., the mean elevation of two AWS and the elevation of THS, respectively. The
 256 values of T_p in different months are obtained by minimizing the error function, i.e.:

257
$$\min : z = \sum (T_i - (T_{oi} + T_p \cdot (H - h)))^2 \quad (2)$$

258 where, i indicates the i^{th} day in the analyzed month, T_i is the observed temperature in AWS,
 259 which is the mean value of the TG AWS and XT AWS in this study.

260 The temperature series data from July 1, 2011 to December 31, 2012 at THS, TG AWS
 261 and XT AWS were used to estimate the temperature lapse rate. The results (Table1) indicate
 262 significant month-to-month variation ranging from $-0.30^\circ\text{C } 100 \text{ m}^{-1}$ in December to -0.86°C
 263 100 m^{-1} in August. To validate the temperature lapse rates, the estimated and observed
 264 temperature data at BT AWS were compared (Fig. 2). We also compared the estimated
 265 temperature by an annual constant lapse rate ($-0.62^\circ\text{C } 100 \text{ m}^{-1}$, a similar value to previous
 266 studies, e.g., Tabony (1985) and Tahir *et al.*(2011)). This constant value is optimized by the
 267 same method in Eqn. (2) but using all daily temperature measurements. Figure 2 indicates that
 268 the monthly lapse rate method performs better than the annual constant rate method at the BT
 269 station for all months throughout the year. Further, the temperature curves estimated by
 270 monthly lapse rates for April to August match the observed ones rather well. Note that the
 271 estimated temperatures tend to underestimate observed ones for the rest of the months, which,
 272 however, will not affect the melt runoff significantly due to the general freezing condition
 273 during this period.

274 **2.2.2 Precipitation Lapse Rate**

275 Based on the precipitation series measured at THS, the monthly precipitation to annual
 276 precipitation ratio (Fig.3) for the study period (2003-2012) indicates that precipitation occurs
 277 mainly in May to September. The lapse rate of precipitation was also estimated monthly, and
 278 a similar procedure as temperature was applied. The different is that the precipitation analysis
 279 was conducted at a weekly rather than daily time step, and the maximum measured
 280 precipitation of the two installed AWS was used instead of the mean value. The analyzed

281 period is limited to the storm rain period (May to September). Other months are not included
282 due to the relatively small precipitation amount. The weekly precipitation lapse rates are
283 listed in Table2. Daily precipitation differences between higher and lower altitudes can be
284 estimated as the weekly precipitation lapse multiplied by the ratio of daily precipitation to the
285 corresponding weekly amount in THS. The precipitation lapse rate was not validated against
286 BT AWS because of significant differences in precipitation distribution between the two
287 basins (i.e., Tailan and Kumalak).

288 **2.2.3 Filtering of MODIS Snow Cover Area Data**

289 Snow cover extent was obtained from MODIS products. The MOD10A2 and MYD10A2
290 products were downloaded from the website <http://reverb.echo.nasa.gov>. In total, we obtained
291 460 eight-day images (two tiles, h23v04 and h24v04) from 2003 to 2012 for each product.
292 Given that the accuracy of the MODIS SCA product is affected by cloud coverage to a
293 significant degree, the remotely sensed images should be filtered to avoid the noise from
294 clouds before using it for hydrological modeling (Ackerman *et al.*, 1998). The following three
295 successive steps are adopted to filter the products based on previous reports (Gafurov and
296 Bardossy, 2009; Wang *et al.*, 2009; Lopez-Burgos *et al.*, 2012):

297 (1) Satellite combination: The snow cover products of two satellites, Terra (MOD10A2)
298 and Aqua (MYD10A2) were combined. As long as the value of a pixel is marked as snow in
299 either satellite, the pixel value is marked as snow.

300 (2) Spatial combination: Inspecting the values of the nearest four pixels around one
301 center pixel marked as cloud, if at least three of the four surrounding pixels are marked as
302 snow, the center pixel is modified as snow.

303 (3) Temporal combination: If one pixel is marked as cloud, its values in the previous and
304 following observations are investigated. If both of the two observed values are snow, then the
305 present value of the same pixel is snow.

306 As an example, the filtered results from year 2004-2005 shown in Fig.4 demonstrate a
307 significant reduction in fluctuation of the SCA products. We find that the lowest values of
308 snow/ice coverage in all years (2003-2012) are relatively stable (from 2003 to 2012 are: 35%,
309 34%, 39%, 36%, 37%, 34%, 41%, 35%, 38%, 39%, showing no obvious trend), which is
310 close to the glacier coverage area (33%) derived from the CGI data mentioned in Sect.2.2. As

311 mentioned before, MODIS snow/ice covered area in later summer is mainly composed of
312 glacier coverage when snow has been melt away completely. The filtered results indicate a
313 relatively stable coverage of glacier in TRB.

314 **2.2.4 Altitudinal Cumulative Melt Curve**

315 The daily temperature of each cell in MODIS SCA images can be estimated by a
316 temperature lapse rate based on its elevation and daily temperature measured at THS. As long
317 as the temperature exceeds a specific threshold value for melt (assumed to be 0°C in this
318 study), a given cell was labeled as an active cell in terms of melt. The land cover type for each
319 cell was classified into glacier, snow, and other land cover according to the CGI and MODIS
320 SCA product. To obtain the area covered by snow only, we subtracted the glacier area in CGI
321 from the SCA (a similar procedure can be found in Luo *et al.*, 2013). When a glacier or snow
322 cover cell is active, it is labeled as a melt cell, and the melt area is computed as the number of
323 active cells multiplied by the area of a cell.

324 Organizing the melt area by elevation from low to high and summing the melt area at
325 each elevation, we can get the altitudinal cumulative melt curve, which can be used to
326 describe the spatiotemporal distribution of melt area. The altitudinal cumulative melt curves
327 calculated from 2003 to 2012 for all months (Fig.5) show that melt mainly occur from May to
328 September, which coincides with the precipitation period. Snowmelt starts at an elevation of
329 approximately 1650 m a.s.l., while glacier melt starts at an elevation of approximately 2950 m
330 a.s.l, which has an important implication for hydrograph partitioning.

331 **3 Methodology**

332 Theoretically, every drop of water in the streamflow comes ultimately from precipitation.
333 Practically, we can consider water sources for runoff generation in mountain areas as mainly
334 consisting of meltwater from snow and glacier, rainwater, and groundwater. Groundwater at
335 the basin scale is recharged by direct infiltration and run-on infiltration of meltwater or
336 rainwater, and it is mainly discharged as baseflow via a subsurface flow path (especially in
337 mountain areas where the large elevation gradient favors baseflow discharge).For the purpose
338 of hydrograph partitioning, we can consider recharge to be a separate water source for
339 streamflow, independent of meltwater and rainwater, which principally forms the baseflow
340 part of a hydrograph. The remaining part of a hydrograph is principally formed by meltwater

341 and rainwater via surface flow path (Blöschl *et al.*, 2013). We develop three indices to
342 indicate the water sources for runoff generation at the daily time scale. The hydrograph is
343 further partitioned into several sub-parts based on the indices values. Each sub-part is
344 dominated by one or more water sources for runoff generation. With the partitioning
345 hydrographic curves, the parameters of hydrological models are correspondingly grouped by
346 runoff sources and calibrated in a stepwise fashion. We use the THREW model coupled with
347 a temperature-index module as an exploratory tool. To better demonstrate usefulness of the
348 proposed methods, only the runoff generation related parameters, which are also significantly
349 sensitive parameters (see Sect.4.6), are calibrated. Other insensitive parameters are fixed at
350 their initial values, specified *a priori* from the literature or by expert knowledge.

351 **3.1 An Index-based Method for Hydrograph Partitioning**

352 In mountain areas, the relative contribution of different runoff water sources to the total
353 streamflow varies throughout the year (Martinec *et al.*, 1982; Dunn and Colohan, 1999; Yang
354 *et al.*, 2007). For the rainwater source, Fig.3 shows that precipitation in TRB presents strong
355 seasonality and primarily concentrates (more than 76%) in the storm rain period from May to
356 September. During the relatively dry period from October to April, mean precipitation gauged
357 at the THS is just 43 mm, while precipitation in the higher mountainous region is mainly
358 snowfall. Therefore, surface runoff induced by rainwater can rarely occur during relative dry
359 period. It is reasonable to assume that the rainwater source can only contribute to the surface
360 runoff part of a hydrograph on the same day during the storm rain period (May to September)
361 except for the baseflow occurring much later.

362 For the meltwater sources, the altitudinal cumulative melt curves (Fig.5) show that the
363 areas experiencing glacier melt and snowmelt change significantly with elevation. Melt of
364 glacier and snow begins at different elevations in different months, i.e., glacier melt can only
365 occur in the areas higher than 2950 m (the lower elevation limit of glacier coverage) while
366 snowmelt can occur in areas higher than 1650 m. It can be deduced that snowmelt generally
367 occurs at lower elevations than glacier melt. Remember that temperature decreases with
368 increase in altitude. There should exist a period of time during which temperature at 1650 m
369 is higher than snowmelt threshold while temperature above 2950 m is lower than glacier
370 threshold and thus snowmelt does occur but glacier melt not.

371 The groundwater source should be a dominant source for the baseflow part of a
 372 hydrograph and, of course, it dominates the recession limb of a hydrograph (part of a
 373 baseflow partition) when no rainfall or melting occurs.

374 Based on the above physical understanding, we can partition the hydrograph using the
 375 following three indices:

376 (1) Date index (D_i): D_i is used to distinguish the dates on which rainfall and thus
 377 possible rainwater directly runoff process occurs. For simplicity, in this study we use
 378 D_i to distinguish dry period and storm rain period and assume no rainfall runoff in
 379 the dry period, i.e.,

$$380 \quad D_i = \begin{cases} 1, & \text{for days in storm rain period from May to September} \\ 0, & \text{for days in relative dry period from October to April} \end{cases} \quad (3)$$

381 (2) Snowmelt index (S_i): S_i indicates whether snowmelt possibly occurs on a
 382 given day:

$$383 \quad S_i = \begin{cases} 1, & \text{for days when temperature at altitude 1650 m is higher than } 0^\circ\text{C} \\ 0, & \text{for other days} \end{cases} \quad (4)$$

384 (3) Glacier melt index (G_i): G_i is used to identify days when glacier melt
 385 possibly occurs:

$$386 \quad G_i = \begin{cases} 1, & \text{for days when temperature at altitude 2950 m is higher than } 0^\circ\text{C} \\ 0, & \text{for other days} \end{cases} \quad (5)$$

387 The hydrograph is then partitioned according to the three indices by using the following
 388 rules:

$$389 \quad Q = \begin{cases} Q_{SB} & \text{for } S_i=0, G_i=0, \text{ and } D_i = 0 \\ Q_{SB} + Q_{SM} & \text{for } S_i=1, G_i=0, \text{ and } D_i = 0 \\ Q_{SB} + Q_{SM} + Q_{GM} & \text{for } S_i=1, G_i=1, \text{ and } D_i = 0 \\ Q_{SB} + Q_{SM} + Q_{GM} + Q_R & \text{for } S_i=1, G_i=1, \text{ and } D_i = 1 \end{cases} \quad (6)$$

390 where, Q is the overall streamflow series, Q_{SB} stands for the baseflow generated by
 391 groundwater source, Q_{SM} for snow meltwater runoff, Q_{GM} for glacier meltwater runoff, and Q_R
 392 for rainwater directly runoff. The partitioning principles are described as follows:

393 (1) Groundwater is the dominant component ($Q=Q_{SB}$) when both melt and rainwater
 394 directly runoff do not occur. This condition is mathematically equivalent to $S_i+G_i+D_i=0$,

395 which requires $S_i=0$, $G_i=0$, and $D_i=0$;

396 (2) Snow meltwater and groundwater are the dominant components ($Q=Q_{SB}+Q_{SM}$) when
397 the temperature is higher than 0 °C at 1650 m a.s.l. and lower than 0 °C at 2950 m a.s.l.
398 (requires $S_i=1$, $G_i=0$, and $D_i=0$);

399 (3) Snow meltwater and glacier meltwater coupled with groundwater dominate
400 ($Q=Q_{SB}+Q_{SM}+Q_{GM}$) on days when the temperature at 2950 m a.s.l. exceeds 0 °C in October to
401 April. This means $G_i=1$, $D_i=0$, and $S_i=1$, noting that S_i must be equal to 1 when $G_i=1$ for the
402 decreasing nature of temperature along altitude;

403 (4) Finally, all sources are mixed ($Q=Q_{SB}+Q_{SM}+Q_{GM}+Q_R$) for other days in the storm
404 rain period (May to September, $D_i=1$). Each category contains days that could be continuous
405 or discontinuous in time and could lie within different weeks due to temporal variability of
406 precipitation and temperature.

407 **3.2 Tsinghua Representative Elementary Watershed Hydrological Model**

408 The Tsinghua Representative Elementary Watershed model (THREW model) used for
409 the hydrological simulation in this study, has been successfully applied in many watersheds in
410 both China and the United States (see Tian *et al.*, 2008, 2012; Li *et al.*, 2012; Liu *et al.*, 2012
411 etc.), including an application to a high mountainous catchment of Urumqi River basin by
412 Mou *et al.* (2008). The THREW model adopts the REW (Representative Elementary
413 Watershed) approach to conceptualize a watershed, where REW is the sub-catchment unit for
414 hydrological modeling. The study basin was divided into several units (REW) based on a
415 digital elevation model. Sub-catchment units were further divided into a surface and
416 sub-surface layer, each layer containing several sub-zones. The sub-surface layer is composed
417 of two zones: saturated zone and unsaturated zone, and the surface layer consists of six zones:
418 vegetated zone, bare soil zone, snow covered zone, glacier covered zone, sub-stream-network
419 zone, and main channel reach; see Tian *et al.* (2006) for further details.

420 The main runoff generation processes simulated by the THREW model include rainfall
421 surface runoff, groundwater baseflow, snowmelt and glacier melt. Rainfall surface runoff is
422 simulated by a Xin'anjiang module, which adopts a water storage capacity curve to describe
423 non-uniform distribution of water storage capacity of a sub-catchment (Zhao, 1992). The
424 storage capacity curve is determined by two parameters (spatial averaged storage capacity W_M

425 and shape coefficient B). Rainfall surface runoff forms on areas where storage is replete.
426 Replete areas are calculated by the antecedent storage and current rainfall. The saturation
427 excess runoff is computed based on water balance. The remainder of rainfall can infiltrate into
428 soil and become additional contributions to groundwater. Groundwater forms baseflow that is
429 separately calculated by two coefficients (K_A and K_D). K_A and K_D are outflow coefficients of
430 groundwater storage. Their sum determines the flow rate of groundwater baseflow and their
431 ratio (K_D/K_A) dominate the proportion of free groundwater storage. Infiltration and storage
432 should have effects on the calibration of the two parameters. The Xin'anjiang module has
433 been successfully applied to the Qiedeke, Kaidu, Manasi and Kahai basins in Tianshan
434 Mountain by different authors (Jiang, 1987; Yang *et al.*, 1987; Mu and Jiang, 2009), which
435 indicates its applicability in our study area.

436 For the simulation of melt processes in this study, the THREW model was modified to
437 couple with the temperature-index method, given the easy accessibility of air temperature data
438 and generally good model performance of the temperature-index model (Hock, 2003; Singh *et al.*,
439 2000). Snow and glacier melt are simulated using separate degree-day factors (snowmelt
440 degree day factor D_s and glacier melt degree day factor D_g). Glacier melt only occurs in
441 glacier area according to CGI, which remains stable during the study period (2003-2012, see
442 discussion in Sect. 2.2.3). Precipitation in the snow and glacier zone is divided into rainfall
443 and snowfall according to two threshold temperature values (0°C and 2.5°C are adopted in
444 this study according to Wu and Li (2007)), i.e., when temperature is higher than 2.5°C , all
445 precipitation is rainfall, when temperature is lower than 0°C , all precipitation is snowfall, and
446 when temperature falls between the two thresholds, precipitation is divided into rainfall and
447 snowfall half by half (a simple division scheme adopted here). Rainfall on glacier areas forms
448 runoff and flows into the stream-network directly without infiltration into soil. Snow water
449 equivalent (SWE) on glacier areas is updated by combining snowfall and snowmelt, and for
450 simplicity, snow is assumed to cover all glacier areas when the corresponding SWE is not
451 zero. Snowmelt in glacier areas is simulated using snow degree-day factor D_s until it melts
452 away completely. Snow cover area in non-glacier area is updated using MODIS data. To be
453 noted, snowfall in each subcatchment is calculated according to the daily precipitation and
454 temperature. And snowmelt is simulated using the degree-day method. However, the snow

455 water equivalent in the snow cover zone is not computed. The existing of snow cover in each
456 subcatchment is only determined by MODIS snow image. When the MODIS image indicates
457 the existing of snow cover and meanwhile the daily temperature is higher than 0°C, then
458 snowmelt will occur, otherwise, snowmelt will not occur. The identification of snow cover by
459 MODIS image is in accordance with the fact that the partitioning of snowmelt dominant
460 hydrograph is based on MODIS snow products. If the existing of snow cover is determined by
461 snow water equivalent, the temperature parameters to calculate snowfall can have significant
462 effects on the estimation of the degree-day factor for snowmelt. To partly reduce this effect,
463 we calibrate the degree-day factor for snowmelt on the basis of MODIS snow cover products.
464 Although in this way, the water balance of snow cover is not taken into account in the snow
465 cover zone, it should not impact the calibration of the degree-day factor for snowmelt. Since
466 MODIS SCA products (i.e., MYD10A2) are available from 2003, the model simulation
467 period is from 2003 to 2012, of which 2003-2007 for calibration and 2008-2012 for
468 evaluation. The time step for simulation is daily.

469 **3.3 Stepwise Calibration of Grouped Parameters Upon Partitioning Curves**

470 Model parameters are grouped *a priori* according to their connection with causal
471 physical mechanisms (see Table 3). According to Xie *et al.* (2004) and Kang *et al.* (1980),
472 parameters that control groundwater baseflow, snowmelt, glacier melt, and rainwater surface
473 runoff should be the most sensitive parameters for the runoff simulation (also see our
474 sensitivity analysis in Sect. 4.6). These parameters are subjected to calibration in this study.
475 They are related to the corresponding hydrograph parts and then calibrated in a stepwise
476 manner: first, groundwater baseflow parameters (K_A and K_D) are estimated based on the Q_{SB}
477 part of the hydrograph. Second, snowmelt degree day factor (D_s) is calibrated upon the
478 $Q_{SB}+Q_{SM}$ part. Third, glacier melt degree-day factor (D_g) is determined according to the
479 $Q_{SB}+Q_{SM}+Q_{GM}$ part. Finally, rainfall surface runoff parameters (B , W_M) are calibrated on days
480 when D_i equals to 1, i.e., the $Q_{SB}+Q_{SM}+Q_{GM}+Q_R$ part of hydrograph.

481 In each step, only the specific parameter group is subjected to calibration. The
482 parameters determined in the previous steps are kept constant, and all other parameters that
483 will be calibrated in the next steps adopt their initial values. As the simulation in each step can,
484 to some degree, be affected by the initial conditions produced in the preceding step, an

485 iterative procedure is implemented to progressively minimize this influence. The parameter
 486 groups are first calibrated based on the corresponding hydrograph parts, and then the stepwise
 487 sequence is repeated until the calibrated parameters converge, i.e., the difference in parameter
 488 values between two contiguous iterations is less than 10%. In each calibration step, we use
 489 $RMSEln$ (Eqn. (7), emphasizing low flow) or $RMSE$ (Eqn. (8), emphasizing high flow) as
 490 objective function for parameter optimization. The remaining, insensitive, parameters are
 491 determined *a priori* according to previous modeling experience (mainly from Sun *et al.*
 492 (2012)) and listed in Table 3. The initial values of the calibrated parameters are also
 493 determined *a priori* according to Sun *et al.* (2012) and Tian *et al.* (2012).

494 The overall streamflow can be simulated with all calibrated parameters, which is
 495 evaluated with NSE and $NSEln$ (logarithm Nash Criterion) values. Given that it is relatively
 496 easier to obtain high evaluation merit values in snowmelt driven basins due to strong
 497 seasonality of streamflow, we further adopt a simple benchmark model (the inter-annual mean
 498 value for every calendar day) to evaluate performance of the proposed method by subtracting
 499 streamflow seasonality. This benchmark model is proposed by Schaeffli and Gupta (2007) for
 500 basins having a relatively constant seasonality. The improvement of a model comparing to the
 501 benchmark model is quantified by the BE , see Eqn. (9) for detail.

$$502 \quad RMSE \ln = \sqrt{\frac{1}{n} \sum_{i=1}^n (\log Q_{obs}(i) - \log Q_{sim}(i))^2} \quad (7)$$

$$503 \quad RMSE = \sqrt{\frac{1}{n} \sum_{i=1}^n (Q_{obs}(i) - Q_{sim}(i))^2} \quad (8)$$

$$504 \quad BE = 1 - \frac{\sum_{i=1}^n (Q_{obs}(i) - Q_{sim}(i))^2}{\sum_{i=1}^n (Q_{obs}(i) - Q_{ben}(i))^2} \quad (9)$$

505 **4 Results and Discussion**

506 **4.1 Partitioning Hydrographic Curves**

507 The hydrograph from 2003 to 2012 was partitioned based on Eqn. (6). In total, we
 508 obtained four kinds of partitioning curves, i.e. Q_{SB} part, $Q_{SB}+Q_{SM}$ part, $Q_{SB}+Q_{SM}+Q_{GM}$ part
 509 and $Q_{SB}+Q_{SM}+Q_{GM}+Q_R$ part. As an example, the partitioning curves in 2003 are shown in Fig.
 510 6, in which the melting period ranges from late February to late November (labeled as red and

511 green dots). Snowmelt (red dots) starts in February and ends in November, while glacier melt
512 (green dots) starts later (March) and stops earlier (October). This melt situation agrees well
513 with the previous studies of Kang *et al.* (1980) and Sun *et al.* (2012). Hydrograph parts
514 dominated by groundwater source mainly fall into December, January and February and are
515 denoted by black dots. The rainwater surface runoff occurs in the storm rain period only (May
516 to September, denoted by blue dots). The total number of days of $Q_{SB}+Q_{SM}$ part from 2003 to
517 2007 is 365, and that of $Q_{SB}+Q_{SM}+Q_{GM}$ part is 249, while the $Q_{SB}+Q_{SM}+Q_{GM}+Q_R$ part
518 occupies 765 days. The numbers of non-melt days (i.e. the Q_{SB} part, due to glacier melt
519 generally occurs in the $Q_{SB}+Q_{SM}+Q_{GM}+Q_R$ part) in the five years are 114, 80, 89, 96, and 68,
520 respectively. Correspondingly, the mean temperatures in those years gauged at the THS are
521 8.9, 10.1, 9.9, 10.4, and 11.3°C, respectively. A lower mean annual temperature causes a
522 longer non-melt period in that year and vice versa. Note that the partitioning curves can be
523 discontinuous in time due to the spatial-temporal variability of temperature.

524 **4.2 Model Calibration by the Stepwise Method**

525 The six key parameters (K_A , K_D , D_s , D_g , W_M , and B) were firstly calibrated by the
526 proposed stepwise and iterative method. To focus on baseflow generated by the groundwater
527 source during the Q_{SB} period, the $RMSEln$ metric that emphasizes low flow is chosen as the
528 evaluation criterion for the calibration of parameters K_A and K_D . Conversely, high flow is our
529 focus for the remaining periods ($Q_{SB}+Q_{SM}$, $Q_{SB}+Q_{SM}+Q_{GM}$, $Q_{SB}+Q_{SM}+Q_{GM}+Q_R$) and the
530 $RMSE$ metric is chosen as the evaluation criterion for calibration of parameters D_s , D_g , and
531 W_M and B . To deal with interaction between steps, an iterative calibration approach was
532 adopted. A total of five iterations was implemented until the parameter estimates became
533 stable; the simulation of each kind of partitioning curve in each step of the last iteration is
534 presented in Fig. 7. The calibrated parameters are shown in Table 4 and the evaluation merits
535 are listed in Table 5.

536 Figure 7a shows that the magnitude of baseflow in Q_{SB} part was captured well at most of
537 the times. The $RMSEln$ merit is 0.302 m³/s, and the parameters K_A and K_D were determined as
538 1.1 and 0.002 respectively. Streamflow in the $Q_{SB}+Q_{SM}$ part is dominated by both snow
539 meltwater and groundwater. The Fig.7b shows that melt peak flow events have also been
540 captured well by a calibrated D_s as 2.5 mm °C⁻¹ day⁻¹ after the determination of K_A and K_D in

541 the first step. For the $Q_{SB}+Q_{SM}+Q_{GM}$ part, glacier meltwater began to control the streamflow
542 in combination with snow meltwater and groundwater. Snowmelt and baseflow were
543 determined *a priori* by previously calibrated parameters. The remaining residual between the
544 simulated and observed discharge can be attributed to glacier melt alone, which was thus used
545 for the calibration of glacier melt factor D_g . The *RMSE* value for this hydrograph partition
546 was optimized as 4.784 m³/s and we obtained a sound simulation by a calibrated D_g as 7.2
547 mm °C⁻¹ day⁻¹ as shown in Fig.7c. During the storm rain periods ($Q_{SB}+Q_{SM}+Q_{GM} +Q_R$ part),
548 rainwater directly runoff is an additional important component of river runoff. Similarly,
549 parameters W_M and B can be calibrated separately after *priori* determination of melt runoff
550 and groundwater baseflow. The simulated *RMSE* value in this period is 12.650 m³/s, with
551 calibrated $W_M=10.50$ cm and $B=0.80$. The overall daily streamflow simulation is obtained by
552 combining the four partitions together (see Figure 8a). The corresponding *NSE* index is 0.881
553 and *NSEln* is 0.929. Generally the results suggest a sound simulation compared to the
554 observation.

555 To be noted, the calibrated values of melt degree day factors D_s (2.5mm °C⁻¹ day⁻¹) and
556 D_g (7.2mm °C⁻¹ day⁻¹) are similar to the values obtained in other studies in Tainshan area, e.g.,
557 D_s is calibrated as 2.5 mm °C⁻¹ day⁻¹ by Liu *et al.* (2012), and D_s and D_g are estimated as 3.1
558 mm °C⁻¹ day⁻¹ and 7.3 mm °C⁻¹ day⁻¹ respectively based on observed mass balance data by Liu
559 *et al.* (1999), which indicates the robustness of our calibration method.

560 **4.3 Comparison to Automatic Calibration Method**

561 For comparison, we also carry out an automatic calibration with the help of the
562 ϵ -NSGAI algorithm, an optimization method developed by Deb *et al.* (2002) and Kollat and
563 Reed (2006). The six parameters were calibrated together and evaluated by *NSE* value of the
564 overall hydrograph. The run time of the automatic algorithm is about 5 weeks (840 hour on a
565 desktop equipped with an Intel Core i7 CPU with 2.8GHz). The *NSE* value for the final
566 optimized parameters is 0.868, and the *NSEln* value is 0.846 (Fig. 8b), both of which are
567 lower than the values obtained by the proposed stepwise method. The parameters calibrated
568 by ϵ -NSGAI are listed in Table 4, and are different from those calibrated by the stepwise
569 method. Specifically, the snowmelt degree-day factor (D_s) and groundwater baseflow
570 parameters (K_A and K_D) obtained by ϵ -NSGAI are 2.03mm °C⁻¹ day⁻¹ and 5.6 and 99.1

571 respectively. The evaluation merits of *RMSE* and *RMSEln* for each partitioning curve are also
572 shown in Table 5. In general, the simulation by the automatic algorithm is not as good as that
573 by the stepwise method, especially for the low and middle flow partitions ($Q_{SB}+Q_{SM}$ and
574 $Q_{SB}+Q_{SM}+Q_{GM}$). This may be due to the tendency of NSE-based automatic calibration to
575 emphasize high flows.

576 To make a further evaluation, a benchmark model suggested by Schaefli and Gupta
577 (2007) is used for the comparison, which simply simulates daily runoff as the inter-annual
578 daily mean value. Simulation results by the benchmark model are shown in the Figure 8c,
579 which shows *NSE* value as 0.815 and *NSEln* value as 0.923. The high *NSE* and *NSEln* values
580 can be attributed to the strong seasonality of stream discharge in the study basin (Schaefli and
581 Gupta, 2007). The *BE* index (Eqn. (9), see Table 5) is used to measure the improvement of
582 simulations by the calibration methods compared to the benchmark model. A positive value
583 for *BE* means that the evaluated method outperforms the benchmark model. Figure 8 shows
584 the simulations of daily streamflow by the three methods (Fig.8a by stepwise calibration
585 method, Fig.8b by automatic calibration method and Fig.8c by benchmark model), which
586 shows better simulation by the two calibration runs with THREW model than the benchmark
587 model (*BE* values are both positive). The stepwise calibration run obtained a *BE* value of
588 0.355, while *BE* of the automatic calibration run is 0.271. The benchmark model describes the
589 mean value of daily discharge on each calendar day. The higher the *BE* value is, the better the
590 seasonal variability of the hydrograph is captured by the evaluation method. The higher *BE*
591 value in the stepwise calibration method can be attributed to the better simulation of middle
592 and low flows which are dominated by groundwater and melt water (Fig.8a). However, *BE*
593 values simulated by two calibrated parameter sets are both relatively low, which is attributed
594 to the poor mimic of the (rapidly rising and falling) peaks.

595 Note that the automatic calibration method based on *NSE* value of the overall
596 hydrograph adopts 1D measurement information to optimize four parameter groups.
597 **Benefitting from the partitioning curves, however, the stepwise calibration method increases**
598 **the dimension of hydrological signature to four. The signature dimension is now equal to the**
599 **number of parameter groups**, and the grouped parameters can be optimized according to their
600 corresponding runoff sources separately. A sound simulation of the overall hydrograph is

601 obtained by the reasonable reproduction of the separate partitioning curves. Therefore,
602 parameters calibrated by the stepwise method are inclined to have more explicit physical
603 basis.

604 In regards to computation efficiency, the stepwise calibration required 385 runs of the
605 model to complete, with each model run taking about 1.5 minutes and the total computation
606 time being about 10 hrs. In contrast, the state-of-the-art automatic calibration algorithm
607 required about 5 weeks of CPU time consumption on a desktop equipped with an Intel Core
608 i7 CPU and 2.8GHz. The comparison indicates that the stepwise calibration method is both
609 more physically based as well as more computationally efficient.

610 It is worth noting, the performance of the automatic calibration algorithm can increase if
611 the algorithm keeps on running, and even be higher than that of the step-wise calibration
612 method. The comparison here is intending to show that the step-wise calibration method
613 based on hydrograph partition can achieve considerable performance more effectively. The
614 automatic algorithm here treats all the parameters equally during the calibration period. Each
615 parameter should be optimized when searching for the optimal parameter set. This searching
616 algorithm hampers the efficiency of the calibration procedure without identifying the
617 dominant sub-periods for different parameters. In the step-wise calibration method, only
618 parameters that are responsible for the simulation of corresponding hydrograph partition are
619 optimized in each step. And also the calibration of parameter by this method reflects the role
620 of each parameter for the basin runoff generation.

621 **4.4 Evaluation for the Stepwise Calibration Method**

622 The parameter set calibrated by the stepwise method is applied to the evaluation period
623 (2008~2012), and the daily discharge simulation is shown in Fig.9a. The evaluation merits are
624 listed in Table 5. The *NSE*, *NSEln* and *RMSE* values for the whole period indicate sound
625 evaluation results but general lower performance compared to calibration period. However,
626 the evaluation results by the stepwise method are still significant better than the benchmark
627 model, which obtained a *NSE* value as low as 0.577 (Fig. 9b and Table 5). The *BE* value in
628 evaluation period by the stepwise calibration method is 0.413. Furthermore, from the partition
629 perspective, the *RMSEln* and *RMSE* values for four partitions in Table 5 show that the low
630 flow simulations (Q_{SB} , $Q_{SB}+Q_{SM}$, and $Q_{SB}+Q_{SM}+Q_{GM}$ parts) are pretty good and even

631 outperform the calibration simulations. The high flow simulation ($Q_{SB}+Q_{SM}+Q_{GM}+Q_R$ part) is,
632 however, insufficient, with $RMSE$ $16.727\text{m}^3/\text{s}$ (compared to $12.65\text{ m}^3/\text{s}$ in calibration period).
633 The lower performance of overall evaluation should be attributed to the insufficiency in storm
634 rain days, especially for some extreme storm events in the summer of 2010 (see Fig. 9a). The
635 underestimation of these events is likely due to inadequate observations of rainfall, which are
636 principally due to the strong spatial variability of rainfall in mountainous areas. It is widely
637 acknowledged that the extreme runoff events are difficult to capture in mountain area, where
638 gauged station is scarce, on the daily scale (Aizen *et al.*, 2000; Jasper *et al.*, 2002). However,
639 the accuracy of our results is similar to Li and Williams (2008) (used SRM model) and Liu *et*
640 *al.*(2012) (who used the MIKE-SHE model) who performed similar work in a basin that is
641 close to TRB in Tianshan Mountains. Their Nash values for daily discharge varied from 0.51
642 to 0.78, and also failed to simulate the peak flows in summer. They also attributed the low
643 efficiency to the heavy precipitation.

644 To further evaluate the robustness of the stepwise calibration method based on
645 partitioning curves, cross validation was implemented. The hydrograph in the evaluation
646 period was partitioned based on dominant runoff sources, as was done in the calibration years
647 2003-2007. We calibrated the model to 2008-2012 and evaluated it for 2003-2007. The new
648 calibrated parameter values are $K_A=0.9$, $K_D=0.003$, $D_s=2.2\text{ mm }^\circ\text{C}^{-1}\text{ day}^{-1}$, $D_g=7.4\text{ mm }^\circ\text{C}^{-1}$
649 day^{-1} , $W_M=10.2\text{cm}$ and $B=0.77$, which are similar to the values calibrated in 2003-2007 listed
650 in Table 4. The NSE , NSE_{ln} and $RMSE$ values for calibration period 2008-2012 and
651 evaluation period 2003-2007 are 0.757, 0.900, $10.892\text{m}^3/\text{s}$ and 0.883, 0.910, $8.589\text{m}^3/\text{s}$,
652 respectively, using this new calibrated parameter set. The simulations of the two periods by
653 cross validation are presented in Fig.9c-d, which shows similar performance by two calibrated
654 parameter sets and further demonstrates the robustness of the proposed stepwise calibration
655 method.

656 **4.5 Sensitivity Analysis on Index-based Partitioning Method**

657 The stepwise calibration method relies heavily on the hydrograph partition for different
658 runoff sources. The indices defined in Sect. 3.1 are keys to identify the dominant days for
659 melt water and rainwater. The definitions for elevation bands for the 0°C Isotherm and for
660 storm rain days in the year producing rainwater runoff should have significant influence on

661 the parameter calibration. In this study, the elevation band of 0 °C Isotherm for snowmelt is
662 fixed and defined as 1650m. This value should have minimal effect on the snowmelt
663 simulation, as the occurrence of snowmelt is actually determined by the MODIS snow cover
664 data. Glacier cover area is assumed as constant, which is very rough for we have only one
665 CGI data. In this section, we define different elevation bands of 0 °C Isotherm for glacier to
666 analyze the effect of glacier area variation on the model calibration. We also select different
667 seasons as the storm rain period to analyze its sensitive effect.

668 According to the CGI data, the glacier area extends from the altitude of 2950m in 2002.
669 Considering the possible variability, we define four different lowest elevation bands for the
670 glacier area (LEG), i.e., -500m (2450m), -200m (2750m), +200m (3150m) and +500m
671 (3450m). As an example, various hydrograph partition patterns in year 2003 are shown in Fig.
672 10. For the storm rain period (SRP), new seasons are defined as April to October, April to
673 September, May to October, and June to August compared to the benchmark period May to
674 September. A new hydrograph partition pattern in year 2003 is also shown in Fig. 10. The left
675 column in Fig. 10 shows that the $Q_{SB}+Q_{SM}+Q_{GM}$ partition becomes longer while the $Q_{SB}+Q_{SM}$
676 partition becomes shorter when the LEG is lower. Therefore, glacier melt starts earlier and
677 ends later in the years with lower LEG. In the right column, the $Q_{SB}+Q_{SM}+Q_{GM}$ partition
678 becomes longer with the shorter SRP, while the variation of the $Q_{SB}+Q_{SM}$ partition can be
679 negligible. Parameters were re-calibrated according to the new partition curves, and the
680 results are shown in Table 6, indicating the increase of degree-day factor for glacier melt (D_g)
681 with the increase of the LEG. The value of D_g is also found to become higher when the SRP
682 falls in the warmer months. The variation of LEG imposes significant impacts on the
683 calibration of D_g , with a result ranging from 5.8 to 8.0mm °C⁻¹ day⁻¹, while the variation of
684 SRP principally impacts the calibration of parameter W_M , with a result ranging from 8.2 to
685 10.5cm. However, the *NSE* values (see Table 6) for different settings show minimal
686 differences. This can be attributed to the fact that parameters are optimized on separate
687 partitioning curves in the stepwise calibration method. Each hydrograph partition can be well
688 simulated by adjusting the parameter values. The partition patterns can influence the value of
689 parameters significantly but only slightly influence the discharge simulation. Among various
690 LEGs, the setting of 2950m leads to the highest *NSE* value. Glacier melt degree day factor (D_g)

691 calibrated with this LEG is $7.2 \text{ mm } ^\circ\text{C}^{-1} \text{ day}^{-1}$, which is very close to the value estimated as
692 $7.3 \text{ mm } ^\circ\text{C}^{-1} \text{ day}^{-1}$ by Liu *et al.*(1999), in which the D_g is estimated according to the observed
693 glacier mass balance data in Tianshan area. This can further demonstrate the reasonability of
694 the assumption in Sect. 3.2 that the glacier area is stable and its lowest elevation is fixed at
695 2950m during the study period. For the various storm rain periods (SRP), when the May to
696 October period is adopted, the discharge simulation is slightly better than the benchmark
697 setting of SRP, i.e. May to September. This phenomenon seems to indicate the importance of
698 precipitation measurement as discussed in Sect. 4.4. With the help of more advanced
699 precipitation measurement, the storm rain period can be determined more precisely to
700 improve the model simulation.

701 To evaluate the relative dominance of multiple runoff sources on the total runoff, we
702 compute their contributions to total runoff by various LEG and SRP in Fig.11. The mean
703 contributions of every runoff source are as follows: groundwater contributes 17%, snow
704 meltwater contributes 16.5%, glacier meltwater contributes 40% and rainwater directly runoff
705 contributes 26.5%. Total melt water (snowmelt and glacier melt) occupies approximately 56.5%
706 and is close to the ratio 63% suggested by Kang *et al.* (1980).

707 **4.6 Sensitivity Analysis on Parameters**

708 The number of parameters to be calibrated is determined by the parameter sensitivity and
709 *a priori* analysis. To evaluate the effect of different parameters on the simulation of different
710 hydrograph partitions, we implemented a simple parameter sensitivity procedure that is
711 carried out by a “one-at-a-time” approach. Parameters from different groups in Table 3 are
712 selected for sensitivity analysis, including saturated hydraulic conductivity for u-zone K_s^u ,
713 saturated hydraulic conductivity for s-zone K_s^s , subsurface flow coefficient K_A and K_D ,
714 manning roughness coefficient for hillslope n^t , spatial heterogeneous coefficient for
715 infiltration capacity α^{IFL} , ground surface depression storage capacity $Fmax^b$, shape coefficient
716 to calculate the saturation excess runoff area from the Xin’anjiang model B , spatial averaged
717 tension water storage capacity in the Xin’anjiang model W_M , glacier degree day factor D_g
718 and snowmelt degree per day factor D_s . Parameter are varied from -50% to +50% of the
719 calibrated values using the stepwise method in Table 4. The relative change (R_{MS}) of
720 simulated measure merits ($RMSEln$ or $RMSE$) for different hydrograph partitions are used to

721 evaluate the sensitivity (Eqn. (10)), where MS is the value of measure merits by the calibrated
 722 parameter, MS_+ is the merits value obtained by the parameter +50% of the calibrated one, and
 723 MS_- is the merits value obtained by the parameter -50% of the calibrated one. The sensitivity
 724 simulation results are shown in Table 7, which demonstrates the dominant control of
 725 parameter K_A , K_D , W_M , B , D_s and D_g . Some parameters have significant effects on simulation
 726 of multi hydrograph partitions. For example, parameters controlling the $Q_{SB}+Q_{SM}+Q_{GM}+Q_R$
 727 period can also have significant effect on the other periods. To minimize this interaction,
 728 iterative calibration was implemented in the calibration procedure. The number of calibrated
 729 parameters is determined as six, which control the main runoff sources (i.e. groundwater
 730 baseflow, snowmelt, glacier melt and rainwater directly runoff). Note that the low dimension
 731 of parameter calibration should not account for the low efficiency of peak flow simulation,
 732 referring to the similar study in Tianshan mountain areas by Li and Williams (2008), and Liu
 733 *et al.*(2012), in which the models have a higher parameter dimension (higher than six), and
 734 the peak flow simulations are still inadequate.

$$735 \quad R_{MS} = \left| \frac{MS_+ - MS_-}{MS} \right| \times 100\% \quad (10)$$

736 **5 Summary and Conclusion**

737 This study proposes diagnostic calibration approach to extracting **hydrological signatures**
 738 from available data series in a mountain area, which can be further used to partition the
 739 hydrograph into dominant runoff sources. The parameters of a hydrological model were
 740 grouped according to runoff sources and then related to the corresponding hydrologic
 741 partitioning curve. Each parameter group was calibrated to improve the simulation of the
 742 corresponding partitioning curve in a stepwise way. In this way, the dimension of
 743 **hydrological signature** is expanded to equal the number of parameter groups. The parameter
 744 uncertainty due to interaction of parameters is reduced via an iterative calibration procedure.
 745 Application to a mountain watershed in the Tianshan Mountain in northwestern China
 746 showed that the approach performed reasonably well. Cross validation and comparison to an
 747 automatic calibration method indicated its robustness.

748 Note that a semi-distributed hydrological model was utilized to illustrate the proposed
 749 diagnostic calibration approach in the high mountainous Tailan River Basin. Glacier mass

750 balance is not simulated in the model and the glacier coverage was kept fixed during the study
751 period, which can be subject to significant change in the context of global warming.
752 According to existing studies (Stahl *et al.*, 2008; Schaefli and Huss, 2011; Jost *et al.*, 2012),
753 glacier mass balance data is useful to constrain the parameter uncertainty for hydrological
754 modeling in a glaciated basin. While arguing that our assumption of unchanged glacier
755 coverage will not weaken the importance of the proposed approach, we acknowledge that an
756 improved model coupled with glacier mass balance equations will improve the accuracy of
757 hydrological simulation aided by glacier mass balance observations. This is left for future
758 research.

759 A prerequisite for the proposed approach is hydrograph partitioning based on dominant
760 runoff sources. The key to the partition procedure is to identify the functional domain of each
761 runoff source from signature information extracted from easily available data. A partition can
762 be achieved in which the relative roles of different runoff sources in the basin runoff vary
763 significantly with time. The mountain watershed is an area in which the runoff sources can be
764 separated by the combination of topography, ground-gauged temperature and precipitation,
765 and remotely sensed snow and glacier coverage. Other areas with strong temporal variability
766 of catchment wetness along with precipitation (e.g., monsoon zones) could also be suitable
767 for the proposed approach. The Dunne runoff is prone to dominate the hydrograph when the
768 catchment is wet and it could switch to Hortonian runoff rapidly under the combination of
769 high evaporative demand and less precipitation, as shown by Tian *et al.* (2012) in the Blue
770 River basin of Oklahoma. This is, however, also left for future research.

771 *Acknowledgments.* We wish to thank Mr. Wang Xinhui for his assistance in collecting
772 hydrometeorology data in the Tailan River basin, and thank Charlie Luce and Viviana
773 Lopez-Burgos who provided great help in MODIS snow coverage product filtering. The
774 authors would also like to thank sincerely two Referees (B. Schaepli and M. Zappa) and Editor
775 Markus Weiler for his careful comments, which improve the quality of manuscript significantly.
776 This study was supported by the National Science Foundation of China (NSFC 51190092,
777 U1202232, 51222901) and the foundation of the State Key Laboratory of Hydroscience and
778 Engineering of Tsinghua University (2012-KY-03, 2014-KY-01). Their support is greatly
779 appreciated.

780 **References**

- 781 Ackerman, S. A., Strabala, K. I., Menzel, W. P., Frey, R. A., Moeller, C. C. and Gumley, L.
782 E.: Discriminating clear sky from clouds with MODIS, *J. Geophys. Res.*,103, 32141-32157,
783 1998.
- 784 Aizen, V., Aizen, E., Glazirin, G. and Loaiciga, H. A.: Simulation of daily runoff in Central
785 Asian alpine watersheds, *J. Hydrol.*, 238, 15-34, 2000.
- 786 Akyurek, Z., Surer, S. and Beser, O.: Investigation of the snow-cover dynamics in the Upper
787 Euphrates Basin of Turkey using remotely sensed snow-cover products and
788 hydrometeorological data, *Hydrol. Process.*,25 (23), 3637-3648, 2011.
- 789 Arnold, J. G. and Allen, P. M.: Automated methods for estimating baseflow and ground water
790 recharge from streamflow records, *Journal of the American Water Resources Association*,
791 35, 411-424, 1999.
- 792 Arnold, J. G., Allen, P. M., Muttiah, R. and Bernhardt, G.: Automated base-flow separation
793 and recession analysis techniques, *Ground Water*, 33, 1010-1018, 1995.
- 794 Beven, K.: Prophecy, reality and uncertainty in distributed hydrological modelling, *Adv.*
795 *Water Resour.*, 16, 41-51, 1993.
- 796 Beven, K.: Equifinality and uncertainty in geomorphological modelling, *The Scientific Nature*
797 *of Geomorphology: Proceedings of the 27th Binghamton Symposium in Geomorphology*,
798 289-313, 1996.
- 799 Beven, K. and Binley, A.: The future of distributed models-model calibration and uncertainty
800 prediction, *Hydrol. Process.*, 6, 279-298, 1992.
- 801 Beven, K. and Freer, J.: Equifinality, data assimilation, and uncertainty estimation in
802 mechanistic modelling of complex environmental systems using the GLUE methodology, *J.*
803 *Hydrol.*,249, 11-29, 2001.
- 804 Blöschl, G., Sivapalan, M., Wagener, T., Viglione, A. and Savenije, H.(Eds.): *Runoff*
805 *Prediction in Ungauged Basins: Synthesis Across Processes, Places and Scales*, Cambridge
806 *Univ. Press*, New York,2013.
- 807 Boyle, D. P., Gupta, H. V. and Sorooshian, S.: Toward improved calibration of hydrologic
808 models: Combining the strengths of manual and automatic methods, *Water Resour. Res.*,
809 36, 3663-3674, 2000.
- 810 Brazil, L.: Multilevel calibration strategy for complex hydrologic simulation models, NOAA
811 *Technical Report*, NWS 42, Fort Collins, 217 pp, 1989.
- 812 Bulygina, N., McIntyre, N. and Wheeler, H.: Conditioning rainfall-runoff model parameters
813 for ungauged catchments and land management impacts analysis, *Hydrol. Earth Syst. Sci.*,
814 13 (6), 893-904, 2009.
- 815 Daly, S. F., Davis, R., Ochs, E. and Pangburn, T.: An approach to spatially distributed snow
816 modelling of the Sacramento and San Joaquin basins, California, *Hydrol. Process*, 14
817 (18S1), 3257-3271, 2000.
- 818 Deb, K., Pratap, A., Agarwal, S. and Meyarivan, T.: A fast and elitist multiobjective genetic
819 algorithm: NSGA-II, *IEEE Transactions on evolutionary computation*, 6, 182-197, 2002.
- 820 Detenbeck, N. E., Brady, V. J., Taylor, D. L., Snarski, V. M. and Batterman, S. L.:
821 Relationship of stream flow regime in the western Lake Superior basin to watershed type
822 characteristics, *J. Hydrol.*, 309, 258-276, 2005.
- 823 Duan, Q., Sorooshian, S. and Gupta, V.: Effective and efficient global optimization for

824 conceptual rainfall-runoff models, *Water Resour. Res.*, 28, 1015-1031, 1992.

825 Dunn, S. M. and Colohan, R. J. E.: Developing the snow component of a distributed
826 hydrological model: a step-wise approach based on multi-objective analysis, *J. Hydrol.*,
827 223, 1-16, 1999.

828 Eder, G., Fuchs, M., Nachtnebel, H. and Loibl, W.: Semi-distributed modelling of the
829 monthly water balance in an alpine catchment, *Hydrol. Process.*, 19, 2339-2360, 2005.

830 Farmer, D., Sivapalan, M. and Jothityangkoon, C.: Climate, soil, and vegetation controls upon
831 the variability of water balance in temperate and semiarid landscapes: Downward approach
832 to water balance analysis, *Water Resour. Res.*, 39, 1035, 2003.

833 Fierz, C., Ribet, P., Adams, E., Curran, A., Fohn, P., Lehning, M. and Pluss, C.: Evaluation of
834 snow-surface energy balance models in alpine terrain, *J. Hydrol.*, 282 (1-4), 76-94, 2003.

835 Gafurov, A. and Bardossy, A.: Cloud removal methodology from MODIS snow cover
836 product, *Hydrol. Earth Syst. Sci.*, 13, 1361-1373, 2009.

837 Gan, T. Y. and Biftu, G. F.: Automatic calibration of conceptual rainfall-runoff models:
838 Optimization algorithms, catchment conditions, and model structure, *Water Resour. Res.*,
839 32, 3513-3524, 1996.

840 Gao, W., Li, Z. and Zhang, M.: Study on Particle-size Properties of Suspended Load in
841 Glacier Runoff from the Tomor Peak, *Arid Zone Research*, 28, 449-454, 2011(in Chinese).

842 Gomez-Landesa, E. and Rango, A.: Operational snowmelt runoff forecasting in the Spanish
843 Pyrenees using the snowmelt runoff model, *Hydrol. Process.*, 16, 1583-1591, 2002.

844 Gupta, H. V., Kling, H., Yilmaz, K. K. and Martinez, G. F.: Decomposition of the mean
845 squared error and NSE performance criteria: Implications for improving hydrological
846 modelling, *J. Hydrol.*, 377, 80-91, 2009.

847 Gupta, H. V., Sorooshian, S. and Yapo, P. O.: Toward improved calibration of hydrologic
848 models: Multiple and noncommensurable measures of information, *Water Resour. Res.*, 34,
849 751-763, 1998.

850 Gupta, V. K. and Sorooshian, S.: Uniqueness and observability of conceptual rainfall-runoff
851 model parameters: The percolation process examined, *Water Resour. Res.*, 19, 269-276,
852 1983.

853 Gupta, V. K. and Sorooshian, S.: The Automatic Calibration of Conceptual Catchment
854 Models Using Derivative-Based Optimization Algorithms, *Water Resour. Res.*, 21,
855 437-485, 1985.

856 Gupta, H. V., Wagener, T. and Liu, Y.: Reconciling theory with observations: elements of a
857 diagnostic approach to model evaluation, *Hydrol. Process.*, 22, 3802-3813, 2008.

858 Gurtz, J., Baltensweiler, A. and Lang, H.: Spatially distributed hydrotope-based modelling of
859 evapotranspiration and runoff in mountainous basins, *Hydrol. Process.*, 13, 2751-2768,
860 1999.

861 Haberlandt, U., Klocking, B., Krysanova, V. and Becker, A.: Regionalisation of the base flow
862 index from dynamically simulated flow components - a case study in the Elbe River Basin,
863 *J. Hydrol.*, 248, 35-53, 2001.

864 Hingray, B., Schaefli, B., Mezghani, A. and Hamdi, Y.: Signature-based model calibration for
865 hydrological prediction in mesoscale Alpine catchments, *Hydrolog. Sci. J.*, 55 (6),
866 1002-1016, 2010.

867 Hock, R.: Temperature index melt modelling in mountain areas, *J. Hydrol.*, 282, 104-115,

868 2003.

869 Hooper, R. P. and Shoemaker, C. A.: A Comparison of Chemical and Isotopic Hydrograph
870 Separation, *Water Resour. Res.*, 22, 1444-1454, 1986.

871 Howard, C.: Revisiting the degree-day method for snowmelt computations – Discussion,
872 *Water Resources Bulletin*, 32 (2), 411-413, 1996.

873 Huss, M., Farinotti, D., Bauder, A. and Funk, M.: Modelling runoff from highly glacierized
874 alpine drainage basins in a changing climate, *Hydrol. Process.*, 22 (19SI), 3888-3902, 2008.

875 Jasper, K., Gurtz, J. and Herbert, L.: Advanced flood forecasting in Alpine watersheds by
876 coupling meteorological observations and forecasts with a distributed hydrological model, *J.*
877 *Hydrol.*, 267 (1-2), 40-52, 2002.

878 Jiang, H. F.: Snow ablation modeling and its application to Qiedeke basin, *Journal of*
879 *Xinjiang Agricultural University*, 1, 67-75, 1987 (in Chinese).

880 Johnston, P. R. and Pilgrim, D. H.: Parameter optimization for watershed models, *Water*
881 *Resour. Res.*, 12, 477-486, 1976.

882 Jost, G., Moore, R. D., Menounos, B. and Wheate, R.: Quantifying the contribution of glacier
883 runoff to streamflow in the upper Columbia River Basin, Canada, *Hydrol. Earth Syst.*
884 *Sci.*, 16, 849-860, 2012.

885 Jothityangkoon, C., Sivapalan, M. and Farmer, D. L.: Process controls of water balance
886 variability in a large semi-arid catchment: downward approach to hydrological model
887 development, *J. Hydrol.*, 254, 174-198, 2001.

888 Juston, J., Seibert, J. and Johansson, P.: Temporal sampling strategies and uncertainty in
889 calibrating a conceptual hydrological model for a small boreal catchment, *Hydrol.*
890 *Process.*, 23 (21), 3093-3109, 2009.

891 Kane, D. L., Gieck, R. E., and Hinzman, L. D.: Snow Modeling at Small Alaskan Arctic
892 Watershed, *Journal of Hydrologic Engineering*, 2 (4), 204-210, 1997.

893 Kang, E., Zhu, S. and Huang, M.: Some Results of the Research on Glacial Hydrology in the
894 Region of MT. Tuomuer, *Journal of Glaciology and Geocryology*, 2, 18-21, 1980(in
895 Chinese).

896 Klok, E. J., Jasper, K., Roelofsma, K. P., Gurtz, J. and Badoux, A.: Distributed hydrological
897 modelling of a heavily glaciated Alpine river basin, *Hydrolog. Sci. J.*, 46 (4), 553-570,
898 2001.

899 Kollat, J. B. and Reed, P. M.: Comparing state-of-the-art evolutionary multi-objective
900 algorithms for long-term groundwater monitoring design, *Adv. Water Resour.*, 29, 792-807,
901 2006.

902 Li, H. Y., Sivapalan, M. and Tian, F. Q.: Comparative diagnostic analysis of runoff
903 generation processes in Oklahoma DMIP2 basins: The Blue River and the Illinois River, *J.*
904 *Hydrol.*, 418, 90-109, 2012.

905 Li, X. G. and Williams M. W.: Snowmelt runoff modelling in an arid mountain watershed,
906 Tarim Basin, China, *Hydrol. Process.*, 22 (19SI), 3931-3940, 2008.

907 Liu, D. F., Tian, F. Q., Hu, H. C. and Hu, H. P.: The role of run-on for overland flow and the
908 characteristics of runoff generation in the Loess Plateau, China, *Hydrolog. Sci. J.*, 57,
909 1107-1117, 2012.

910 Liu, S. Y., Xie, Z. C., Wang, N. L. and Ye, B. S.: Mass balance sensitivity to climate change:
911 a case study of glacier no. 1 at Urumqi riverhead, Tianshan mountains, China, *Chin. Geogr.*

912 Sci., 9, 134-140, 1999.

913 Liu, T., Willems, P., Feng, X. W., Li, Q., Huang, Y., Bao, A. M., Chen, X., Veroustraete, F.
914 and Dong, Q. H.: On the usefulness of remote sensing input data for spatially distributed
915 hydrological modelling: case of the Tarim River basin in China, *Hydrol. Process.*, 26 (3),
916 335-344, 2012.

917 Lopez-Burgos, V., Gupta, H. V. and Clark, M.: A probability of snow approach to removing
918 cloud cover from MODIS Snow Cover Area products, *Hydrol. Earth Syst. Sci. Discuss*, 9,
919 13693-13728, 2012.

920 Luo, Y., Arnold, J., Liu, S., Wang, X. and Chen, X.: Inclusion of glacier processes for
921 distributed hydrological modeling at basin scale with application to a watershed in
922 Tianshan Mountains, northwest China, *J. Hydrol.*, 477, 72-85, 2013.

923 Martinec, J., Oeschger, H., Schotterer, U. and Siegenthaler, U.: Snowmelt and groundwater
924 storage in alpine basin, In *Hydrological Aspects of Alpine and High Mountain Areas*,
925 Wallingford, United Kingdom: IAHS Press, 169–175, 1982.

926 McCuen, R. H.: *Hydrologic analysis and design*, Prentice Hall, New Jersey pp.355-360, 1989.

927 Mendoza, G. F., Steenhuis, T. S., Walter, M. T. and Parlange, J. Y.: Estimating basin-wide
928 hydraulic parameters of a semi-arid mountainous watershed by recession-flow analysis, *J.*
929 *Hydrol.*, 279, 57-69, 2003.

930 Mou, L., Tian, F., Hu, H. and Sivapalan, M.: Extension of the Representative Elementary
931 Watershed approach for cold regions: constitutive relationships and an application, *Hydrol.*
932 *Earth Syst. Sci.*, 12, 565-585, 2008.

933 Mu, Z. X. and Jiang, H. F.: Establishment of snowmelt type Xin'anjiang watershed model
934 based on digital elevation model, *Journal of Xinjiang Agricultural University*, 5 (32), 75-80,
935 2009 (in Chinese).

936 Nash, J. E. and Sutcliffe, J. V.: River flow forecasting through conceptual models part I — A
937 discussion of principles, *J. Hydrol.*, 10, 282-290, 1970.

938 Nathan, R. J., McMahon, T. A.: Evaluation of automated techniques for base flow and
939 recession analyses, *Water Resour. Res.*, 26, 1465-1473, 1990.

940 Nejadhashemi, A. P., Shirmohammadi, A., Sheridan, J. M., Montas, H. J. and Mankin, K. R.:
941 Case Study: Evaluation of Streamflow Partitioning Methods, *J. Irrig. Drain. Eng.*, 135,
942 791-801, 2009.

943 Pellicciotti, F., Brock, B., Strasser, U., Burlando, P., Funk, M. and Corripio, J.: An enhanced
944 temperature-index glacier melt model including the shortwave radiation balance:
945 development and testing for Haut Glacier d'Arolla, Switzerland, *Journal of Glaciology*, 51
946 (175), 573-587, 2005.

947 Pinder, G. F. and Jones, J. F.: Determination of the ground-water component of peak
948 Determination of the ground-water component of peak discharge from the chemistry of
949 total runoff, *Water Resour. Res.*, 5, 438-445, 1969.

950 Rango, A. and Martinec, J.: Application of a Snowmelt-runoff Model Using Landsat Data,
951 *Nord. Hydrol.*, 10, 225-238, 1979.

952 Richter, B. D., Baumgartner, J. V., Powell, J. and Braun, D. P.: A method for assessing
953 hydrologic alteration within ecosystems, *Conservation Biology*, 10, 1163-1174, 1996.

954 Schaeffli, B. and Gupta, H. V.: Do Nash values have value, *Hydro. Process.*, 21 (15),
955 2075-2080, 2007.

956 Schaeffli, B., Hingray, B., Niggli, M. and Musy, A.: A conceptual glacio-hydrological model
957 for high mountainous catchments, *Hydrol. Earth Syst. Sci.*,9 (1-2), 95-109, 2005.

958 Schaeffli, B. and Huss, M.: Integrating point glacier mass balance observations into hydrologic
959 model identification, *Hydrol. Earth Syst. Sci.*,15,1227-1241,2011.

960 Shamir, E., Imam, B., Gupta, H. V. and Sorooshian, S.: Application of temporal streamflow
961 descriptors in hydrologic model parameter estimation, *Water Resour. Res.*, 41, W06021,
962 doi:10.1029/2004WR003409, 2005a.

963 Shamir, E., Imam, B., Morin, E., Gupta, H. V. and Sorooshian, S.: The role of hydrograph
964 indices in parameter estimation of rainfall-runoff models, *Hydrol. Process.*,19, 2187-2207,
965 2005b.

966 Shen, Y., Liu, S., Ding, Y. and Wang, S.: Glacier Mass Balance Change in Tailanhe River
967 Watersheds on the South Slope of the Tianshan Mountains and its impact on water
968 resources, *Journal of Glaciology and Geocryology*, 25, 124-129, 2003(in Chinese).

969 Shi, Y.: Concise Glacier Inventory of China, Shanghai Popular Science Press., Shanghai,
970 China, 2008(in Chinese).

971 Singh, P., Kumar, N. and Arora, M.: Degree-day factors for snow and ice for Dokriani
972 Glacier, Garhwal Himalayas, *J. Hydrol*, 235, 1-11, 2000.

973 Sivapalan, M., Bloschl, G., Zhang, L. and Vertessy, R.: Downward approach to hydrological
974 prediction, *Hydrol. Process.*,17, 2101-2111, 2003.

975 Sorooshian, S. and Gupta, V. K.: Automatic calibration of conceptual rainfall-runoff
976 models-the question of parameter observability and uniqueness, *Water Resour. Res.*, 19,
977 260-268, 1983.

978 Spear, R. C. and Hornberger, G. M.: Eutrophication in peel inlet—II. Identification of critical
979 uncertainties via generalized sensitivity analysis, *Water Research*,14,43-49,1980.

980 Stahl, K., Moore, R. D., Shea, J. M., Hutchinson, D. and Cannon, A. J.: Coupled modelling of
981 glacier and streamflow response to future climate scenarios, *Water Resour. Res.*,44,2008.

982 Sun, M., Yao, X., Li, Z. and Li, J.: Estimation of Tailan River Discharge in the Tianshan
983 Mountains in the 21st Century, *Advances on Climate Change Research*, 8, 342-349,
984 2012(in Chinese).

985 Swamy, A. N. and Brivio, P. A.: Modelling runoff using optical satellite remote sensing data
986 in a high mountainous alpine catchment of Italy, *Hydrol. Process.*, 11 (11), 1475-1491,
987 1997.

988 Tabony, R. C.: The variation of surface temperature with altitude, *Meteorological Magazine*,
989 114, 37-48, 1985.

990 Tahir, A. A., Chevallier, P., Arnaud, Y., Neppel, L. and Ahmad, B.: Modeling
991 snowmelt-runoff under climate scenarios in the Hunza River basin, Karakoram Range,
992 Northern Pakistan, *J. Hydrol*, 409, 104-117, 2011.

993 Tian, F. Q., Hu, H. P. and Lei, Z. D.: Thermodynamic watershed hydrological model:
994 Constitutive relationship, *Science in China, Ser. E-Technological Sciences*, 51, 1353-1369,
995 2008.

996 Tian, F., Hu, H., Lei, Z. and Sivapalan, M.: Extension of the Representative Elementary
997 Watershed approach for cold regions, *Hydrol. Earth Syst. Sci.*, 10, 619-644, 2006.

998 Tian, F. Q., Li, H. Y. and Sivapalan, M.: Model diagnostic analysis of seasonal switching of
999 runoff generation mechanisms in the Blue River basin, Oklahoma, *J. Hydrol*, 418, 136-149,

1000 2012.

1001 Van Griensven, A. and Bauwens, W.: Multiobjective autocalibration for semidistributed
1002 water quality models, *Water Resour. Res.*, 39, 1348, 2003.

1003 Van Straten, G. T. and Keesman, K. J.: Uncertainty propagation and speculation in projective
1004 forecasts of environmental change: A lake-eutrophication example, *J. Forecast.*, 10,
1005 163-190, 1991.

1006 Vivoni, E. R., Entekhabi, D., Bras, R. L. and Ivanov, V. Y.: Controls on runoff generation and
1007 scale-dependence in a distributed hydrologic model, *Hydrol. Earth Syst. Sci.*, 11,
1008 1683-1701, 2007.

1009 Vrugt, J. A., Gupta, H. V., Bastidas, L. A., Bouten, W. and Sorooshian, S.: Effective and
1010 efficient algorithm for multiobjective optimization of hydrologic models, *Water Resour.*
1011 *Res.*, 39, 1214, 2003a.

1012 Vrugt, J. A., Gupta, H. V., Bouten, W. and Sorooshian, S.: A Shuffled Complex Evolution
1013 Metropolis Algorithm for Optimization and Uncertainty Assessment of Hydrological
1014 Model Parameters, *Water Resour. Res.*, 39, 1201, doi:10.1029/2002WR001642, 8., 2003b.

1015 Wang, X. W., Xie, H. J., Liang, T. G. and Huang, X. D.: Comparison and validation of
1016 MODIS standard and new combination of Terra and Aqua snow cover products in northern
1017 Xinjiang, China, *Hydrol. Process.*, 23, 419-429, 2009.

1018 Westerberg, I. K., Guerrero, J. L., Younger, P. M., Beven, K. J., Seibert, J., Halldin, S., Freer,
1019 J. E. and Xu, C. Y.: Calibration of hydrological models using flow-duration curves, *Hydrol.*
1020 *Earth Syst. Sci.*, 15 (7), 2205-2227, 2011.

1021 Wu, J., L. L.: A rain-on-snow mixed flood forecast model and its application, *Engineering*
1022 *Journal of Wuhan University*, 40, 20-23, 2007 (in Chinese).

1023 Xie, C., Ding, Y., Liu, S. and Han, H.: Analysis on the Glacial Hydrological Features of the
1024 Glaciers on the South Slope of Mt. Tuomuer and the Effects on Runoff, *Arid Land*
1025 *Geography*, 27, 570-575, 2004 (in Chinese).

1026 Yadav, M., Wagener, T. and Gupta, H.: Regionalization of constraints on expected watershed
1027 response behavior for improved predictions in ungauged basins, *Adv. Water Resour.*, 30,
1028 1756-1774, 2007.

1029 Yang, D. Q., Zhao, Y. Y., Armstrong, R., Robinson, D. and Brodzik, M. J.: Streamflow
1030 response to seasonal snow cover mass changes over large Siberian watersheds, *J. Geophys.*
1031 *Res.*, 112, F02S22F2, 2007.

1032 Yang, X. S., Jiang, H. F., Huang, C. R., Zheng, Z., and Yong, G.: An applied study on the
1033 snowmelt type of Xin'anjiang watershed model at the Kaidu river basin, *Journal of*
1034 *Xinjiang Agricultural University*, 4, 82-90, 1987 (in Chinese).

1035 Yilmaz, K. K., Gupta, H. V. and Wagener, T.: A process-based diagnostic approach to model
1036 evaluation: Application to the NWS distributed hydrologic model, *Water Resour. Res.*,
1037 44, W09417, doi:10.1029/2007WR006716, 2008.

1038 Zhang, Z. X., Wagener, T., Reed, P. and Bhushan, R.: Reducing uncertainty in predictions in
1039 ungauged basins by combining hydrologic indices regionalization and multiobjective
1040 optimization, *Water Resour. Res.*, 44 (W00B04), doi:10.1029/2008WR006833, 2008.

1041 Zhao, R. J.: The Xin'anjiang model applied in China, *J. Hydrol.*, 135, 371-381, 1992.

1042

Table1. Estimated monthly temperature lapse rate in the TRB

Month	Temperature lapse rate ($^{\circ}\text{C}/\text{day}/100\text{ m}$)
January	-0.38
February	-0.38
March	-0.66
April	-0.76
May	-0.80
June	-0.78
July	-0.82
August	-0.86
September	-0.66
October	-0.60
November	-0.54
December	-0.30
Annual	-0.62

1043

1044

Table 2. Estimated week-precipitation lapse rate in storm rain months

Month	Precipitation lapse rate (mm/week/ 100 m)
May	1.63
June	1.69
July	3.14
August	2.40
September	2.28

1045

1046
1047

Table 3. Grouped parameters in the THREW model. Parameters subjected to calibration are highlighted in red.

Category	Symbol	Unit	Description	Value
Subsurface	K_s^u	m s ⁻¹	Saturated hydraulic conductivity for u-zone	1.25E-05
	K_s^s	m s ⁻¹	Saturated hydraulic conductivity for s-zone	1.25E-05
	K_A	-	Coefficient used to calculate subsurface flow	Calibrated
	K_D	-	Coefficient used to calculate subsurface flow	Calibrated
Routing	n^t	-	Manning roughness coefficient for hillslope, obtained from the literature according to land use and vegetation type	1.50E-01
	n^r	-	Similar to n^t , roughness coefficient for channel	3.00E-01
Infiltration	α^{EFL}	-	Spatial heterogeneous coefficient for exfiltration capacity	1.00E+00
	α^{IFL}	-	Spatial heterogeneous coefficient for infiltration capacity	1.50E+00
Interception	$F \max^b$	m	Ground surface depression storage capacity	0.00E+00
	α^{vb}	m	Maximum rainfall depth a single leaf can intercept and hold	1.00E-05
Rainfall runoff	B	-	Shape coefficient to calculate the saturation excess runoff area from the Xin'anjiang model	Calibrated
	W_M	cm	Spatial averaged tension water storage capacity in the Xin'anjiang model	Calibrated
Melt	D_g	mm °C ⁻¹ day ⁻¹	Glacier melt degree day factor	Calibrated
	D_s	mm °C ⁻¹ day ⁻¹	Snowmelt degree day factor	Calibrated

1048

1049

Table 4. Calibrated parameters by the stepwise and automatic methods

Parameter	Stepwise Calibrated	Automatic Calibrated
K_A	1.1	5.6
K_D	0.002	99.1
$D_s(\text{mm } ^\circ\text{C}^{-1} \text{ day}^{-1})$	2.5	2.03
$D_g(\text{mm } ^\circ\text{C}^{-1} \text{ day}^{-1})$	7.2	7.52
$W_M(\text{cm})$	10.5	11.9
B	0.80	0.62

1050

Table 5. Evaluation merits for the stepwise and automatic calibration methods

Merits	Calibration period	Calibration period	Calibration period	Evaluation period	Evaluation period
	Automatic method	Stepwise method	Benchmark model	Stepwise method	Benchmark model
$RMSEln(Q_{SB}, m^3/s)$	0.352	0.302	-	0.213	-
$RMSE(Q_{SB}+Q_{SM}, m^3/s)$	2.807	1.811	-	1.762	-
$RMSE(Q_{SB}+Q_{SM}+Q_{GM}, m^3/s)$	6.079	4.784	-	4.558	-
$RMSE(Q_{SB}+Q_{SM}+Q_{GM}+Q_R, m^3/s)$	13.245	12.650	-	16.727	-
NSE	0.867	0.881	0.815	0.752	0.577
$NSEln$	0.841	0.929	0.923	0.894	0.844
$RMSE (m^3/s)$	8.990	8.459	10.534	11.021	14.381
BE	0.271	0.355	-	0.413	-

1053 Table 6. Sensitive analysis of the calibrated parameters on lowest elevation band for glacier
 1054 area (LEG) and storm rain period (SRP). *NSE* is the Nash Sutcliffe Efficiency value for the
 1055 calibration period.

	LEG(a.s.l. m)	$D_s(\text{mm/d/}^\circ\text{C})$	$D_g(\text{mm/d/}^\circ\text{C})$	$W_M(\text{cm})$	B	K_A	K_D	NSE
	3450	2.2	8.0	10.1	0.70	0.7	0.002	0.870
	3150	2.5	7.9	10.1	0.75	0.7	0.002	0.871
SRP:	2950	2.5	7.2	10.5	0.80	1.1	0.002	0.881
May. To Sep.	2750	3.0	6.8	10.2	0.75	1.0	0.002	0.880
	2450	2.8	5.8	10.0	0.78	0.8	0.002	0.876
	SRP	$D_s(\text{mm/d/}^\circ\text{C})$	$D_g(\text{mm/d/}^\circ\text{C})$	$W_M(\text{cm})$	B	K_A	K_D	NSE
	Jun. to Aug.	2.9	7.5	8.2	0.75	0.9	0.002	0.871
	May. to Oct.	2.8	6.9	9.4	0.76	0.8	0.002	0.882
LEG=2950m	May. to Sep.	2.5	7.2	10.5	0.80	1.1	0.002	0.881
	Apr. to Sep.	2.2	7.1	8.3	0.75	0.9	0.002	0.878
	Apr. to Oct.	2.6	6.9	9.4	0.77	1.1	0.002	0.881

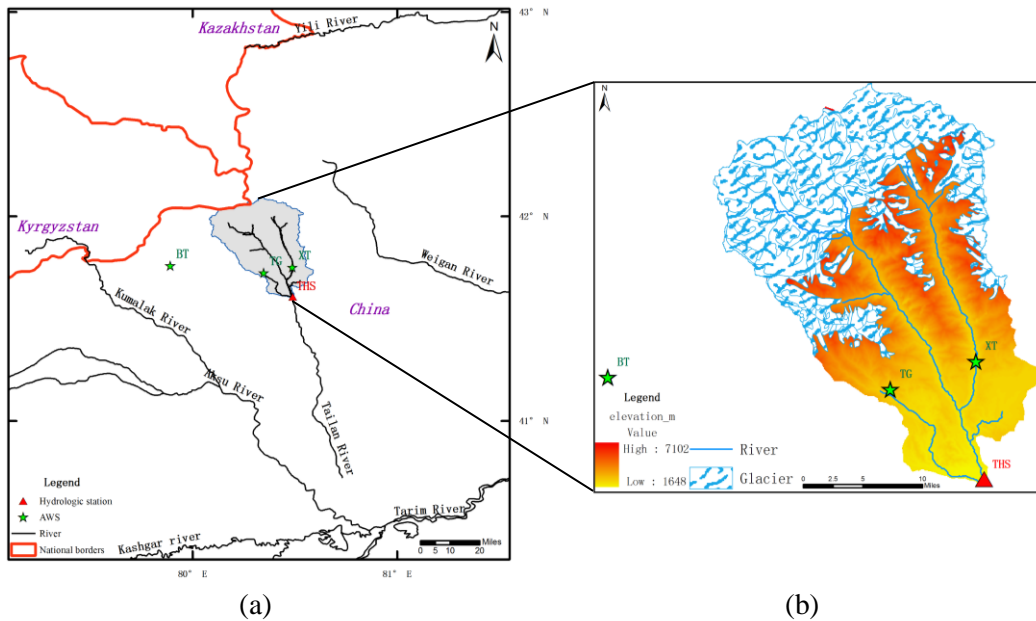
1056

1057
1058

Table 7. R_{MS} (%) for parameter sensitivity (R_{MS} values indicating the most sensitive parameters are labeled in bold and red)

Merits	Subsurface				Routing	Infiltration	Interception	Rainfall Runoff		Melt	
	K_s^u	K_s^s	K_A	K_D	n^t	α^{IFL}	$F \max^b$	W_M	B	D_s	D_g
<i>RMSE</i> _{ln} (Q_{SB})	9.70	11.14	38.44	44.39	15.70	0.12	0.08	1.07	18.51	7.53	2.88
<i>RMSE</i> ($Q_{SB}+Q_{SM}$)	0.32	0.40	11.91	0.06	9.35	0.47	0.14	8.27	25.14	51.22	0.69
<i>RMSE</i> ($Q_{SB}+Q_{SM}+Q_{GM}$)	0.22	0.21	0.62	0.64	10.00	0.17	0.25	7.92	0.29	26.28	40.79
<i>RMSE</i> ($Q_{SB}+Q_{SM}+Q_{GM}+Q_R$)	0.17	0.85	0.57	0.97	1.84	0.08	0.06	19.35	22.48	10.78	11.57

1059

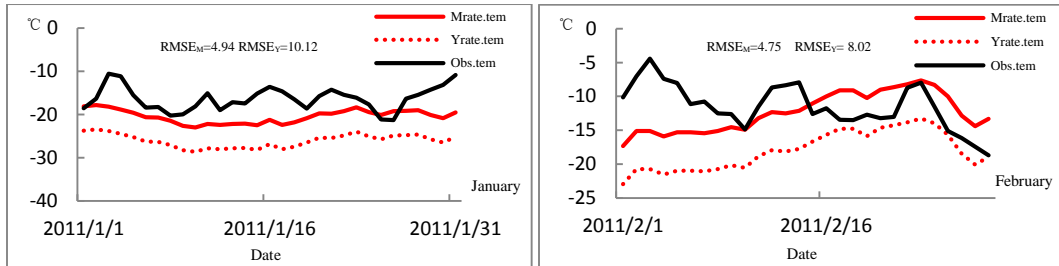


1060
 1061
 1062
 1063
 1064
 1065
 1066
 1067
 1068

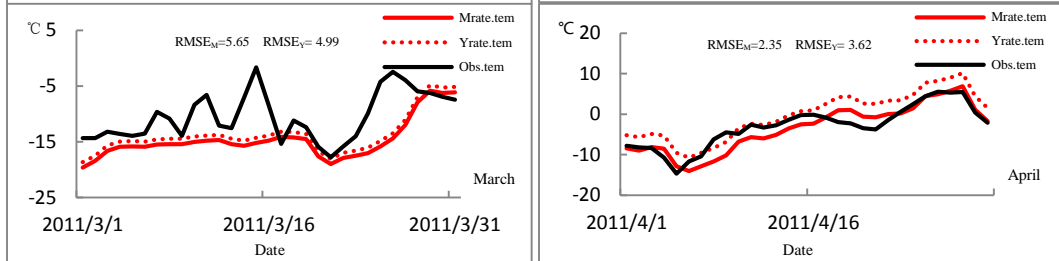
(a) (b)

Figure 1. Location of the Tailan River basin in Xinjiang Uygur Autonomous Region, China. Two automatic weather stations (TG at 2381 m a.s.l. and XT at 2116 m a.s.l.) were set up in upstream mountain area in July, 2011. Additionally, the BT weather station (3950 m a.s.l.) located in the adjacent Kumalak River basin was used to validate the estimated temperature lapse rates. The Tailan Hydrologic Station (THS) has gauged streamflow data at the catchment outlet since 1957(a). Glacier occupies approximately 33% of the total basin area (b).

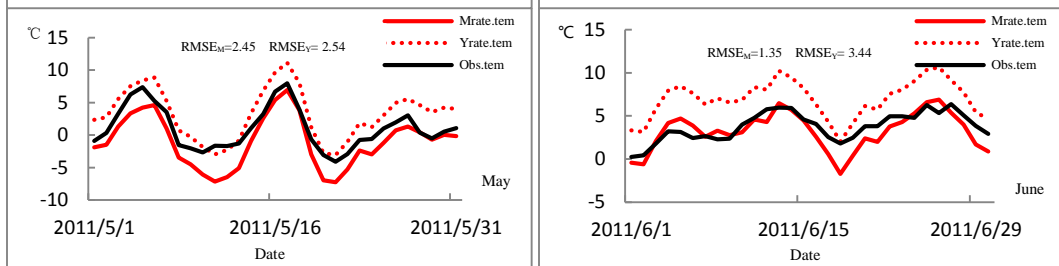
1069



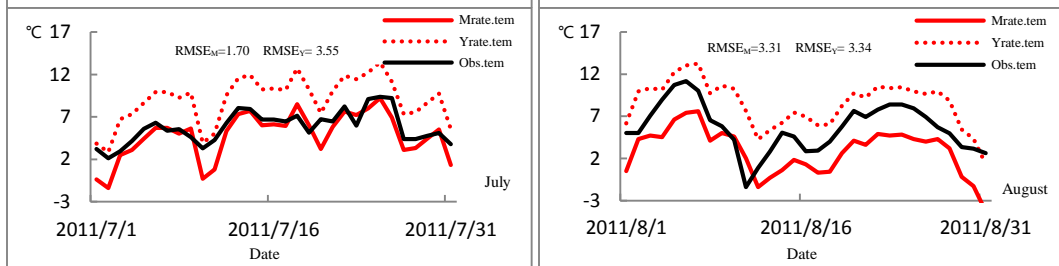
1070



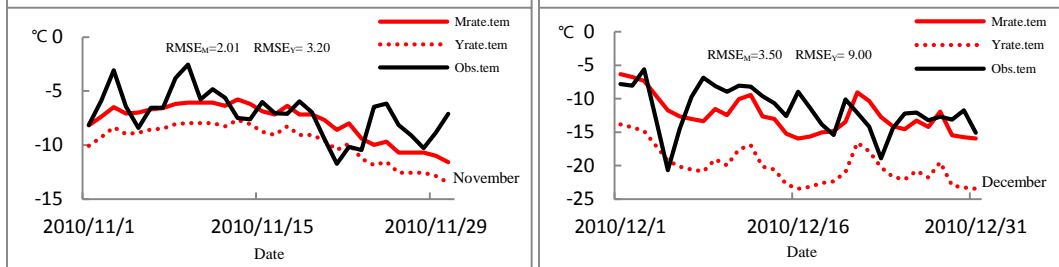
1071



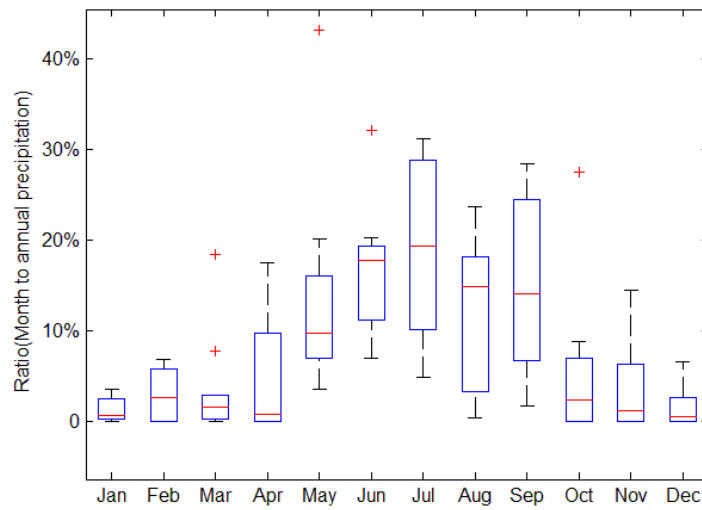
1072



1073

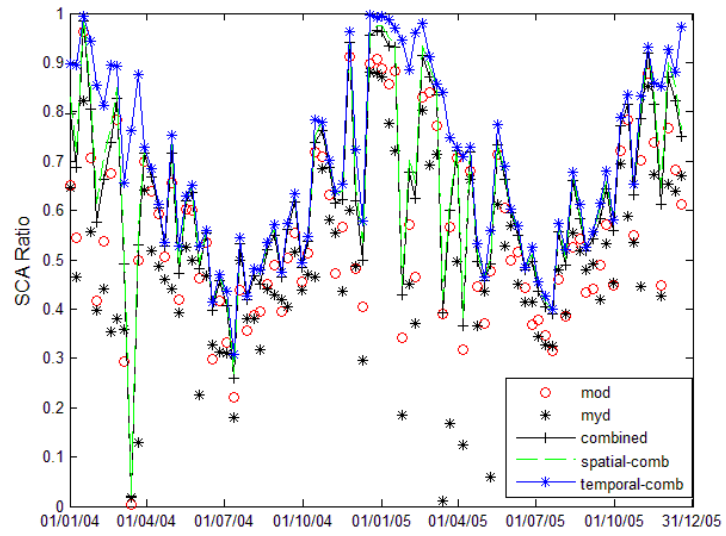


1074 Figure 2. Evaluation of the estimated temperature lapse rate at the BT station. The black solid
 1075 line is the observed temperature series at BT (Obs.tem); the red solid line is the estimated
 1076 temperature by monthly lapse rate (Mrate.tem).The red dotted line indicates the estimated
 1077 temperature based on annual constant rate (Yrate.tem). The goodness of fit between the
 1078 observed and estimated temperature is measured by $RMSE_M$ for monthly lapse rate and
 1079 $RMSE_Y$ for annual constant rate, respectively. The temperature series in September and
 1080 October are absent at BT.



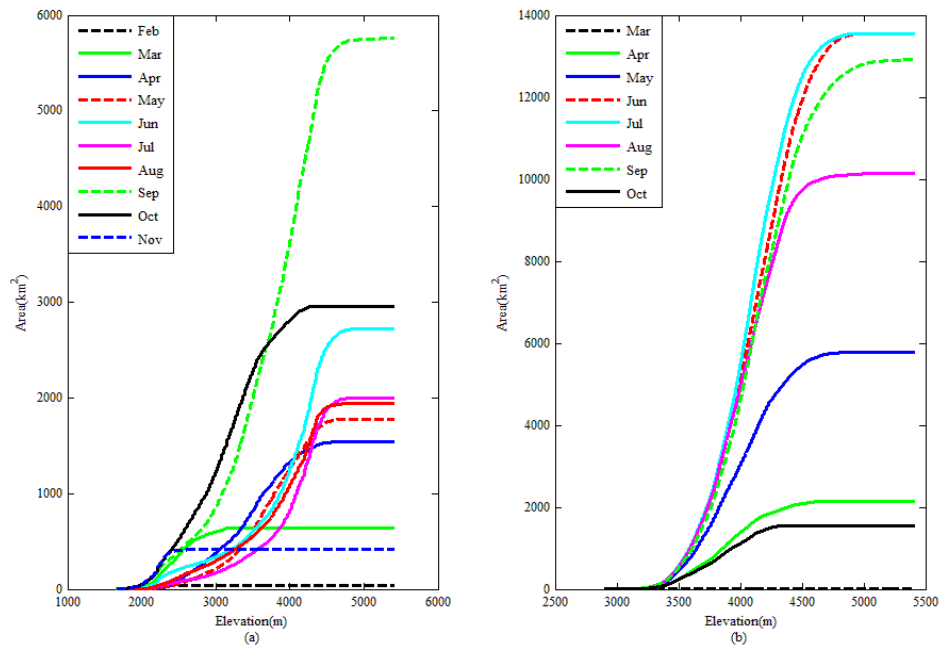
1081

1082 Figure 3. Proportion of monthly precipitation to annual amount (2003~2012). The red line in
 1083 each box represents the median value for each month from 2003 to 2012. Red crosses indicate
 1084 abnormal values that exceed 1.5 times the inter quartile range.



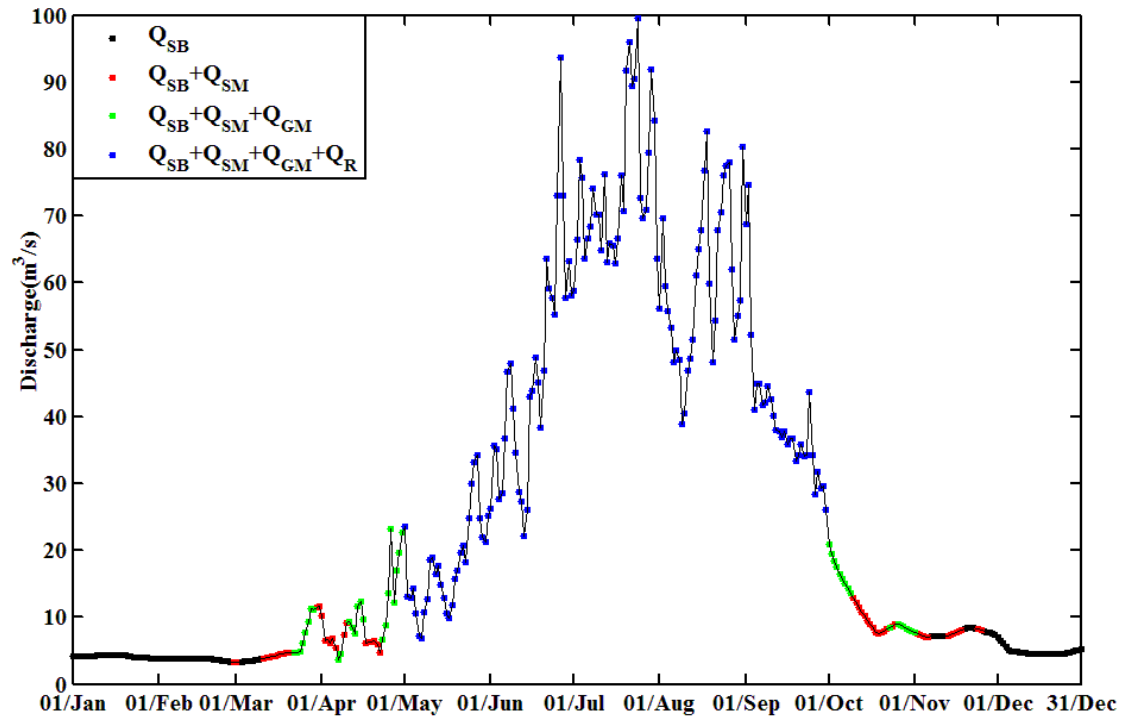
1085
 1086
 1087
 1088
 1089

Figure 4. Filtered MODIS eight-day snow-cover products (2004-2005). The term ‘mod’ is the snow cover area from MOD10A2 products, ‘myd’ is MYD10A2 products, ‘combined’ is the combined result from step1, ‘spatial-comb’ from step2 and ‘temporal-comb’ from step3. See Sect. 2.2.3 for details.



1090
 1091
 1092
 1093
 1094
 1095

Figure 5. Altitudinal Cumulative Melt Curve. (a) Cumulative monthly snowmelt area distribution by elevation (2003~2012). (b) Cumulative monthly glacier melt area distribution by elevation (2003~2012). The snowmelt areas in December and January and the glacier melt areas in November, December, January and February are zero and are not shown in this figure.



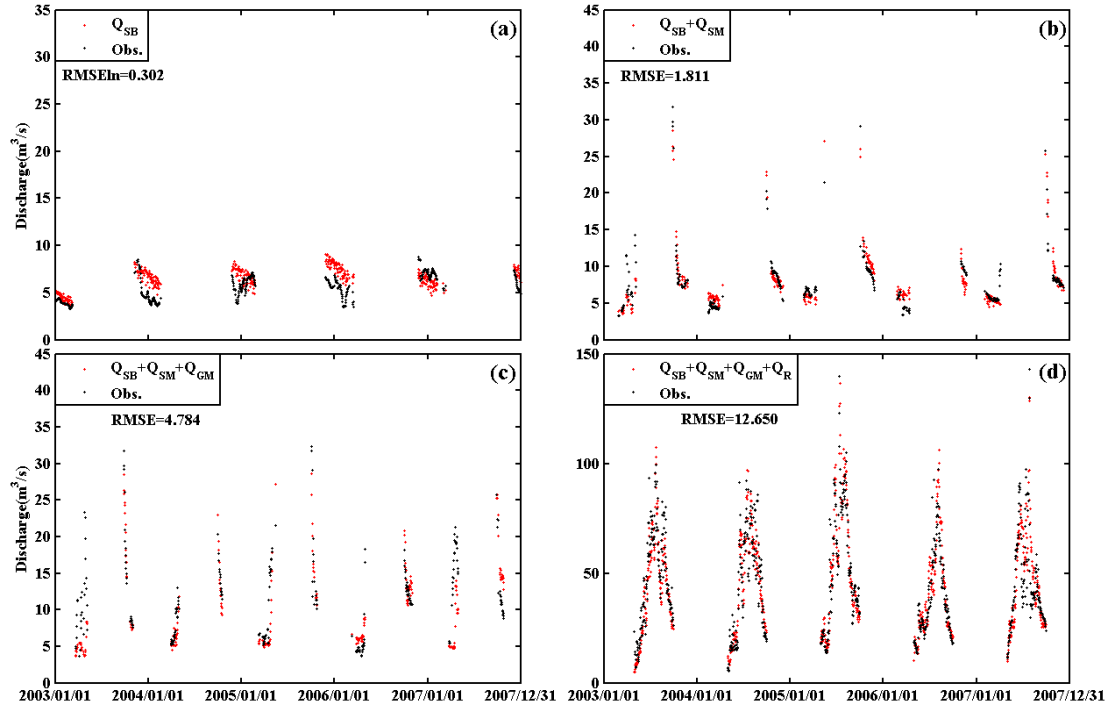
1096

1097

1098

1099

Figure 6. Hydrograph partition in 2003. Q_{SB} stands for subsurface baseflow generated by groundwater, Q_{SM} and Q_{GM} for snow meltwater and glacier meltwater respectively, and Q_R for rainwater directly runoff.



1100

1101

1102

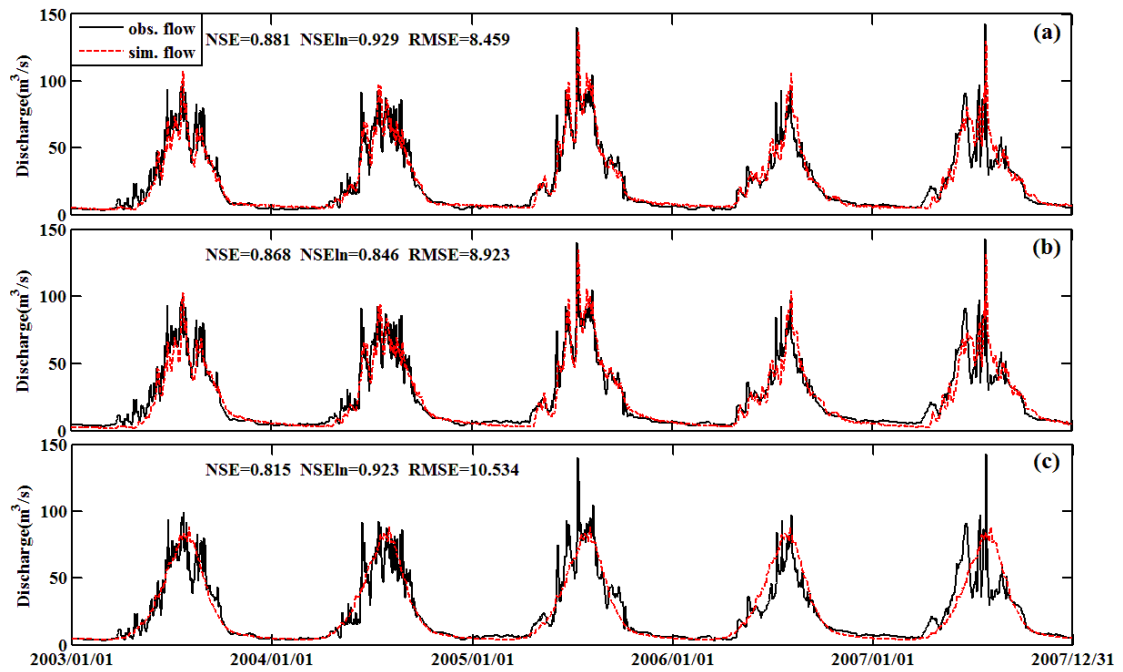
1103

1104

1105

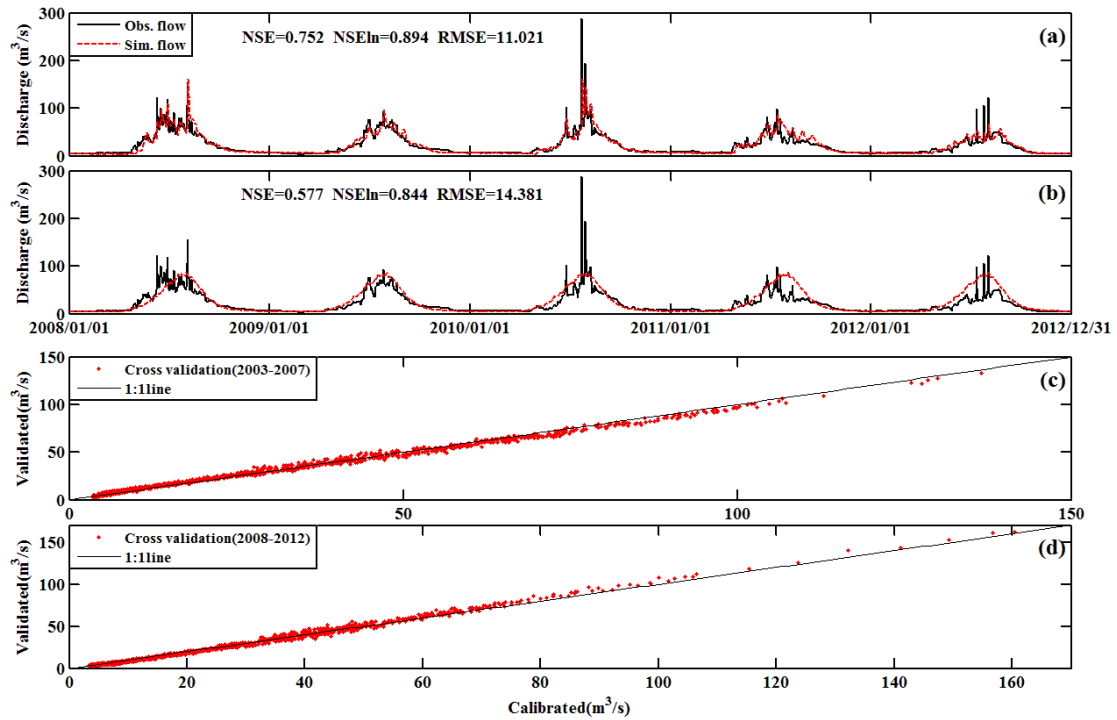
1106

Figure 7. Stepwise calibration of grouped parameters upon partitioning curves. (a) Partitioning curves after calibrating K_A and K_D upon Q_{SB} . (b) Partitioning curves after calibrating D_s upon $Q_{SB}+Q_{SM}$. (c) Partitioning curves after calibrating D_g upon $Q_{SB}+Q_{SM}+Q_{GM}$. (d) Partitioning curves after calibrating W_M and B upon $Q_{SB}+Q_{SM}+Q_{GM}+Q_R$. The goodness of fit between observed and simulated discharge is measured by $RMSEln$ (for Q_{SB} part) or $RMSE$ (for other parts).



1107
 1108
 1109
 1110

Figure 8. Simulation of daily streamflow by different methods from 2003 to 2007. (a) by the proposed stepwise method, (b) by the automatic calibration method, and (c) by the benchmark model. The performance of the simulations is measured in *NSE*, *NSEln* and *RMSE*.



1111

1112

1113

1114

1115

1116

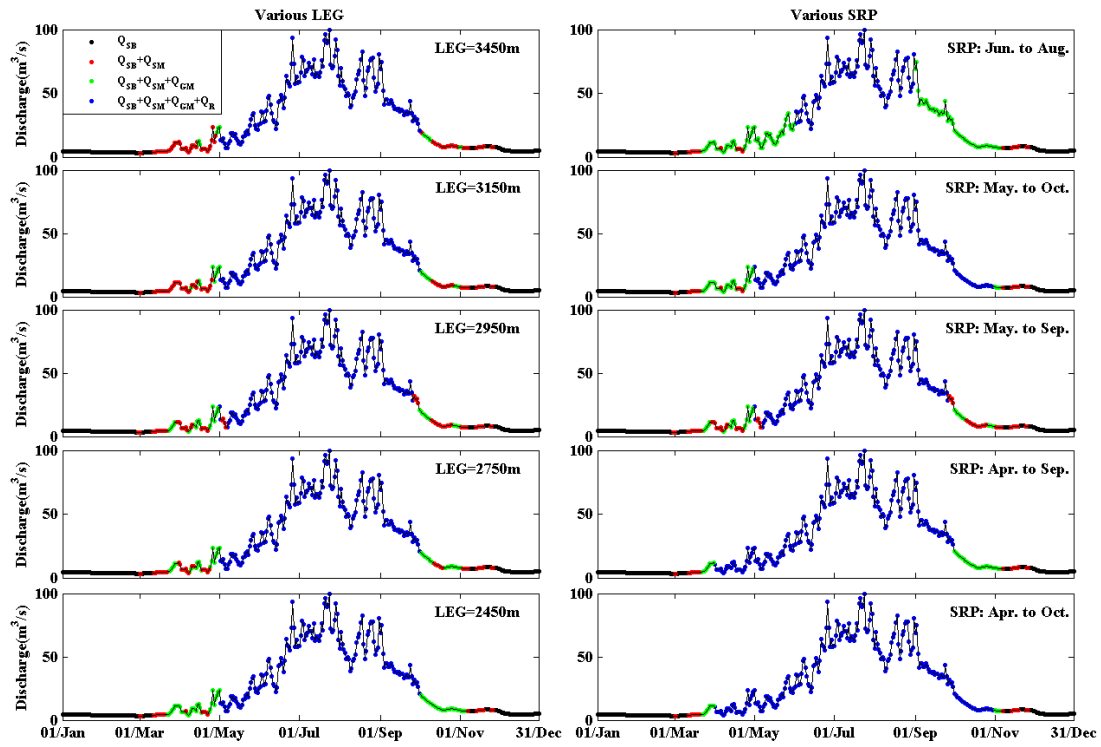
1117

1118

1119

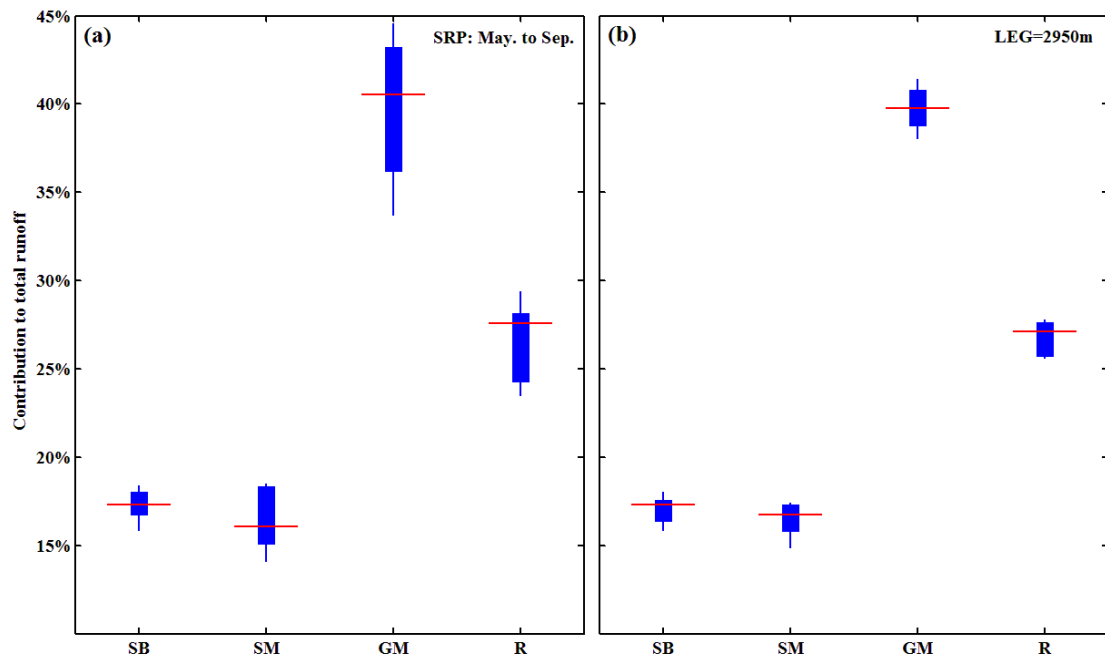
1120

Figure 9. Evaluation of the stepwise calibration method. (a) discharge simulation in evaluation period 2008 to 2012 using the stepwise calibrated parameters in calibration period 2003 to 2007. (b) discharge simulation in evaluation period 2008 to 2012 by the benchmark model. (c) Cross validation simulation of daily discharge in 2003-2007. x-coordinate presents the simulated daily discharges by parameters calibrated in period 2003-2007. y-coordinate presents the simulated daily discharges by parameters calibrated in period 2008-2012. (d) Cross validation simulation of daily discharge in 2008-2012. x-coordinate presents the simulated daily discharges by parameters calibrated in period 2008-2012. y-coordinate presents the simulated daily discharges by parameters calibrated in period 2003-2007.



1121
 1122
 1123
 1124
 1125

Figure 10. Sensitivity analysis for hydrograph partition. The first column is the hydrograph partition pattern using different lowest elevation band of the glacier area (LEG). The second column is the hydrograph partition pattern using different storm rain period (SRP).



1126

1127

1128

1129

1130

1131

1132

1133

Figure 11. Sensitivity analysis on the contributions of different runoff sources to total runoff. (a) is the contribution pattern under different lowest elevation band of glacier area (LEG), where the storm rain period (SRP) is fixed as May to September. (b) is the contribution pattern under different SRPs, where the LEG is fixed as 2950m. The red line stands for the mean contribution for each runoff source, and the top/bottom end of each plot presents the highest/lowest contribution ratio. SB is groundwater baseflow, SM is snowmelt, GM is glacier melt and R is rainwater directly runoff.